

TNO Defence Research

AD-A273 752



TNO F'

Labor:

Oude Wa
2597 AK The Hague
P.O. Box 96864
2509 JG The Hague
The Netherlands

Fax +31 70 328 09 61
Phone +31 70 326 42 21

93-0756

TNO-report

copy no.

FEL-93-A058

title

Results from the VISA project

①
DTIC
ELECTED
DEC 15 1993
S P D

author(s):

G.J. Kunz

TDCK RAPPORTENCENTRALE

Frederikkazerne, gebouw 140
v/d Burchlaan 31 MPC 16A
TEL. : 070-3166394/6395
FAX. : (31) 070-3166202
Postbus 90701
2509 LS Den Haag TDCK

classification

classified by : W. Pelt

classification date : September 1, 1993

title : ongerubriceerd

abstract : ongerubriceerd

report text : ongerubriceerd

appendices A-F : ongerubriceerd

93-30327
19/01

All rights reserved.

No part of this publication may be reproduced and/or published by print, photoprint, microfilm or any other means without the previous written consent of TNO.

In case this report was drafted on instructions, the rights and obligations of contracting parties are subject to either the 'Standard Conditions for Research Instructions given to TNO', or the relevant agreement concluded between the contracting parties.

Submitting the report for inspection to parties who have a direct interest is permitted.

© TNO

no. of copies : 45

no. of pages : 78 (including appendices,
excluding RDP and distribution list)

no. of appendices : 6

All information which is classified according to Dutch regulations shall be treated by the recipient in the same way as classified information of corresponding value in his own country. No part of this information will be disclosed to any party. The classification designation ONGERUBRICEERD is equivalent to UNCLASSIFIED.

Approved for public release
Distribution: *REDACTED*

Netherlands organization for applied scientific research

TNO Defence Research consists of:
the TNO Physics and Electronics Laboratory,
the TNO Prins Maurits Laboratory and the
TNO Institute for Perception.



93 12 14 06 1

The Standard Conditions for Research Instructions given to TNO, as filed at the Registry of the District Court and the Chamber of Commerce in The Hague shall apply to all instructions given to TNO.

**Best
Available
Copy**

report no. : FEL-93-A058
title : Results from the VISA project

author(s) : G.J. Kunz
Institute : TNO Physics and Electronics Laboratory

date : August 1993
NDRO no. : A90K703
no. in pow '93 : 715

Research supervised by : C.W. Lamberts
Research carried out by : G.J. Kunz

ABSTRACT (ONGERUBRICEERD)

A small lidar system has been used to measure the vertical structure of the atmospheric extinction in a dune area bordering The Hague (The Netherlands), at about 2.6 km from the North Sea. The atmospheric optical properties at this location are determined by a mixture of industrial, urban, rural and marine aerosols, which composition depends on the air mass history. The measurements were made unattended, around the clock, five days a week. About 250 extinction profiles were recorded every day. This report reviews the data base obtained and presents some selected results. The lidar system is described briefly. Factors influencing the accuracy of the inversion of lidar signals are discussed.

DTIC QUALITY INSPECTED

Accesion For	
NTIS	CRA&I <input checked="" type="checkbox"/>
DTIC	TAB <input type="checkbox"/>
Unannounced <input type="checkbox"/>	
Justification	
By	
Distribution /	
Availability Codes	
Dist	Avail add/or Special
A-1	

rapport no. : FEL-93-A058
titel : Resultaten van het VISA project

auteur(s) : ir. G.J. Kunz
instituut : Fysisch en Elektronisch Laboratorium TNO

datum : augustus 1993
hdo-opdr.no. : A90K703
no. in lwp '93 : 715

Onderzoek uitgevoerd o.l.v. : Drs. C.W. Lamberts
Onderzoek uitgevoerd door : Ir. G.J. Kunz

SAMENVATTING (ONGERUBRICEERD)

Een klein lidarsysteem is ingezet voor het meten van de vertikale atmosferische extinctie profielen in de duinen aan de rand van Den Haag (Nederland) op een afstand van ca. 2,6 km van de Noordzee. De optische eigenschappen van de atmosfeer aldaar worden bepaald door een combinatie van industriële, stedelijke, natuurlijk continentale en marine aerosolen, afhankelijk van de historie van de luchtmassa. Het gehele proces van meten, data opslag en data verwerking vond continu en automatisch plaats gedurende vijf dagen per week. Per dag werden ongeveer 250 extinctie profielen gemeten. Dit rapport geeft een overzicht van de verkregen gegevens. Een selectie van de resultaten wordt gepresenteerd. Het gebruikte lidarsysteem zal in het kort worden beschreven. Factoren die de nauwkeurigheid beïnvloeden van de inversie van lidarsignalen, worden besproken.

CONTENTS

ABSTRACT	2	
SAMENVATTING	3	
LIST OF SYMBOLS	6	
1	INTRODUCTION	7
2	LIDAR SYSTEM	9
3	INVERSION METHOD	12
3.1	Introduction	12
3.2	Inversion of horizontally measured signals	14
3.3	Inversion of vertically measured signals	17
4	DESCRIPTION OF THE DATA BASE	19
5	INVERTED DATA	21
5.1	Analysis of the horizontal measurements	21
5.2	Analysis of vertical measurements	32
5.3	Statistical review of the vertical extinction	45
6	DISCUSSION AND CONCLUSIONS	52
REFERENCES	55	
APPENDIX A: RANGE OF LIDAR SYSTEMS		
APPENDIX B: CALIBRATION OF THE LOG UNIT		
APPENDIX C: EFFECTS OF THE TRIGGER INACCURACY		

APPENDIX D: EFFECTS OF THE TRANSFER ACCURACY OF THE LOG UNIT

APPENDIX E: DEFINITION OF THE PARAMETERS IN THE DATA BASE

APPENDIX F: SOME RESULTS OF THE SODAR SYSTEM

LIST OF SYMBOLS

A = area of the receiver in km^2
c = speed of light in km/s
D = sensitivity of the receiver in V/W
E_l = energy of the laser in J
K₁ = lidar system constant in $\text{W}\cdot\text{km}^3$
K_{1'} = lidar system constant including the system noise in km^3
L₁ = intercept of the transfer of logarithmic amplifiers in V
L₂ = slope of the transfer of logarithmic amplifiers in V
P_{d(R)} = lidar return on the detector in W
P_n = noise equivalent power of the receiver in W
R = range in km
S(R) = range corrected lidar return in $\text{W}\cdot\text{km}^2$
T_{opt} = transmission of the optics [-]
U_{l(R)} = lidar return at the input of the receiver in V
U_{o(R)} = lidar return at the output of the log unit in V
U_r = reference voltage of 1 V
Z = altitude in km
 α = extinction coefficient in km^{-1}
 β = backscatter coefficient in km^{-1}
 Γ = time constant of a first order electrical filter in s

1

INTRODUCTION

In the period January 1985 to August 1986, vertical extinction profiles of the atmosphere were measured with an automatic lidar system (optical radar) at the TNO Physics and Electronics Laboratory (52°.07'.43" N; 04°.19'.40" E). The location is indicated in Figure 1.1. The system was mounted in a cabin on the roof of the institute, about 15 m above ground level and pointing in a northern direction over the dunes. In principle, an extinction profile was measured every 6 minutes, 5 days a week. Each profile measurement was preceded by one or more horizontal measurements, to determine the horizontal extinction- and backscatter coefficients. Meteorological parameters were recorded in combination with the lidar data. Cloud cover and precipitation were recorded during working hours (when possible). Cloud base height was inverted from the lidar data. Results were presented in Kunz, 1990. In the first few months of the project also a sodar (acoustic radar) was operated but the results were unsatisfactory to continue these measurements.

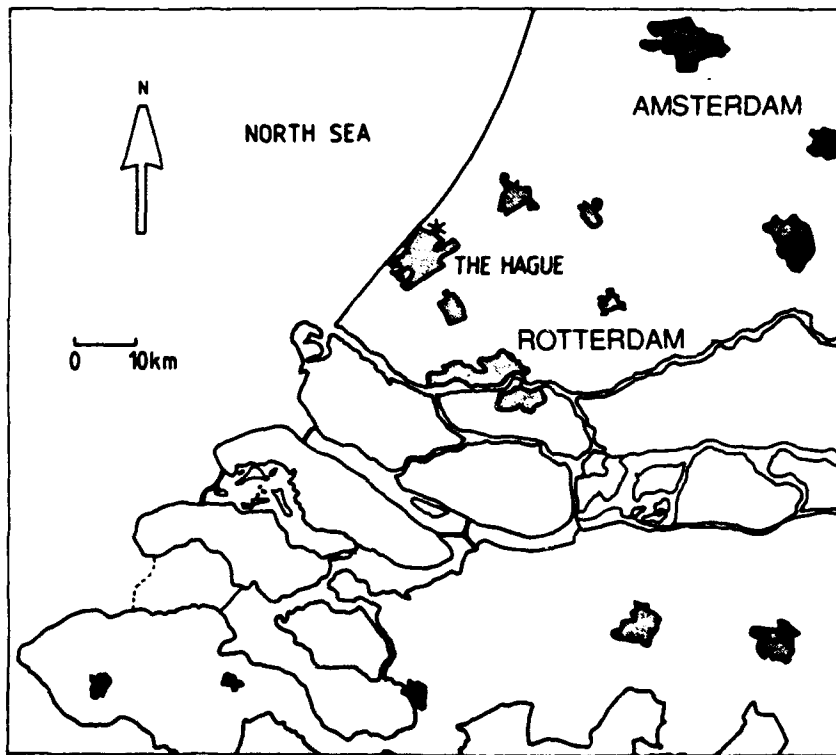


Figure 1.1: Schematic map of the region. The measurement site is indicated by a '*'. Large industrial areas are dotted.

The lidar operated automatically under control of an HP-85 personal computer. The meteorological station was operated with a PET-4000 Commodore Business Computer. Both systems were programmed in BASIC. The lidar signals were processed to obtain the horizontal backscatter- and extinction coefficients (at a level of 15 m altitude) and to obtain the vertical extinction profiles using the forward integration method (Kunz, 1983), see also Chapter 3. The inverted results were stored instead of the raw data. The main reason for this was the limited data storage capacity at that time. In a later stage, the data was converted to IBM-PC format for analysis. Afterward, the lidar and meteorological data were merged into a data base which finally comprised about 23,000 records. This data base provides a unique source for correlation of lidar-measured extinction, backscatter and vertical profiles with the actual meteorological conditions to determine statistical relations between these parameters. Furthermore, the path-integrated extinction can be determined as a function of elevation angle. Slant-path atmospheric extinction plays an important role in models for predicting the performance of electro-optic sensors.

This report describes the lidar system, its calibration and the inversion techniques applied. Factors are discussed which influence the accuracy of the calculated extinction- and backscatter coefficients at low altitudes. An overview of the acquired data base and some selected results are presented and discussed.

2

LIDAR SYSTEM

The TNO Mini-Lidar, shown in Figure 2.1, is a modified laser range finder, developed by the (Dutch) Oldelft Optical Industries (presently named: Delft Electro Optics) as a military laser range finder at the end of the sixties. The powerful laser (100 mJ) and large telescope (74 mm diameter) made the system attractive for modification to a lidar system. The system appeared to be very reliable and has been in operation by TNO-FEL since 1982. It was used both for the semi-continuous measurements during the 2-year VISA project described in this report, as well as during several national and international field experiments on land and over sea. The heart of the Mini-Lidar is a Nd:Glass laser with a rotating prism as Q-switch. The specifications of the lidar are summarized in Table 2.1.



Figure 2.1: TNO Mini Lidar

Table 2.1: Properties of the TNO Mini-Lidar

Transmitter:	
wavelength	1060 nm
energy	50 mJ
pulse duration	30 ns
beam divergence	1 mrad
repetition rate	6 ppm

Receiver:	
diameter telescope	74 mm
focal length	655 mm
RCA C30916 APD (diam.)	1.5 mm
sensitivity @ 1060 nm	12 A/W
color filter RG 830	3 mm
sensitivity	19.3 kV/W (50 Ω)
noise level	0.16 mV ($= 8.3 \cdot 10^{-9}$ W)

Laser Energy

The energy of the laser was measured with three different energy meters. The calibration differences between the meters were less than 2 %. The variation of the laser energy, over 200 shots, was less than 3.3 %. It is assumed that the influence of the energy variation over the measurement periods is negligible. During the project, the laser energy was measured daily and used to calibrate the backscatter measurements.

Sensitivity of the Receiver

The accuracy of the receiver has been tested with a calibrated light emitting diode (LED, 1060 nm and with a power level of 194 nW; Kunz, 1988 and 1989). The emitted light was collimated to fill the field of view of the receiver.

Range of the Lidar

In general, the range of a lidar depends on the properties of the system (e.g. laser energy, receiver diameter and noise of the detector) and on the actual weather condition. For our Mini-Lidar, the

theoretical maximum range is about 1.3 km, in a homogeneous atmosphere with an extinction of 0.4 km^{-1} . In a molecular (Rayleigh) atmosphere the maximum range is about 450 m. The method for calculating the maximum range of lidar systems in a homogeneous atmosphere, is outlined in Appendix A. In cases of an inhomogeneous atmosphere, the range depends on the structure and cannot be predicted *a priori*.

Beam Direction

The slant path direction of the beam in the Mini-Lidar can be controlled via the internal mirror, from an angle of about -10° to about $+33^\circ$ with respect to the horizon. To reach a maximum altitude with the system, an external mirror under 45° was applied during the first few months of the experiments. However, during periods of precipitation this resulted in erroneous signals caused by scattering at the droplets on the mirror. Therefore it was decided to apply only the internal mirror of the system, giving up the altitude advantage for all-weather operations.

Pre-processing

A logarithmic amplifier (Analog Modules LA-90-P) has been used to suppress the dynamic range of the measured signals. This unit has a logarithmic transfer over the first 80 dB of the input signal strength ($0 \text{ dB} = 5 \text{ V}$) and a constant transfer for smaller input signals ($U_i < 5 \cdot 10^{-4} \text{ V}$). The results of the calibration and some other properties of this unit are described in Appendix B.

Data Recording and Processing

The transient recorder was designed and constructed in-house at the beginning of the project because at that time no instruments were commercially available with the desired accuracy, resolution and sample rate. The resolution of the transient recorder was 9 bits and the sample rate was 16 MHz. The trigger accuracy was better than 8 ns to improve the timing accuracy. Errors in the calculated backscatter- and extinction coefficients, caused by small time shifts of the lidar signal, are described in Appendix C. An HP-85 personal computer controlled the lidar system and processed all data.

3

INVERSION METHOD

3.1 Introduction

This paragraph describes in short the model of the lidar signal and the methods used to invert the signals. A comprehensive discussion on this subject can be found in the literature (e.g., Klett 1983, Kunz 1983). Some special topics are discussed more extensively because they have a large impact on the accuracy of the results and have not been described elsewhere.

The general model for lidar signals is given by the following equation:

where:

$$P_d(R) = E_1 \cdot \frac{c}{2} \cdot \frac{\beta(R)}{4\pi} \cdot \frac{A}{R^2} \cdot T_{opt} \cdot \text{EXP} \left\{ -2 \cdot \int_0^R \alpha(x) \cdot dx \right\}, \quad R > 0 \quad (3.1)$$

A	=	area of the receiver in km ²
c	=	velocity of light in km/s
E ₁	=	laser energy in J
P _d (R)	=	lidar return on the detector in W
R	=	range in km
$\beta(R)$	=	backscatter coefficient in km ⁻¹
T _{opt}	=	transmission of the optics
$\alpha(R)$	=	spatial extinction coefficient in km ⁻¹

The duration of the laser pulse does not appear in this formula but must be short in comparison with the smallest range to be observed. The receiver and the transmitter field of views are assumed to have complete overlap.

The output of the receiver in volts is:

$$U_1(R) = D \cdot P_d(R) \quad (3.2)$$

where:

$$\begin{aligned} U_1(R) &= \text{output of the receiver in V} \\ D &= \text{sensitivity of the photo detector in V/W} \end{aligned}$$

Throughout the project, the lidar signals were pre-processed with an analog logarithmic amplifier to compress the large dynamic range of the signals. Thus, the signals could be recorded with a transient recorder with a smaller dynamic range (at the cost of the reliability of very low extinction values). The properties of the logarithmic amplifier are described in Appendix B. The output signal of the logarithmic amplifier can be described by:

$$U_o(R) = L_1 + L_2 \cdot \ln[U_1(R) / U_r] \quad (3.3)$$

where:

$$\begin{aligned} L_1 &= \text{intercept of the transfer in V} \\ L_2 &= \text{slope of the transfer in V} \\ U_o(R) &= \text{output voltage of the log-amplifier in V} \\ U_r &= \text{reference voltage of 1 V} \end{aligned}$$

Division by U_r is only a formal action to render the argument of the log function dimensionless.

Lidar signals can be divided in two classes, i.e. from a homogeneous atmosphere and from an inhomogeneous atmosphere. It is assumed that the lowest layer in the atmosphere is well mixed (over the range of the lidar) which results in a homogeneous distribution of the aerosols. When the atmosphere is sensed in the vertical direction, however, the structure will generally be inhomogeneous.

The purpose of lidar is to determine the atmospheric backscatter- and extinction coefficients. In principle, these two quantities cannot simply be determined with one single system. However, in a homogeneous situation it is possible to determine these two quantities because the strength of the lidar signal is a measure for the backscatter and the time behaviour gives the extinction (see section 3.2). In situations of an inhomogeneous atmosphere the amplitude and the time behaviour of the lidar signal are determined by the spatial properties of both the extinction and the backscatter coefficients. In that case, additional information (a relation between extinction and backscatter as well as a boundary condition) is required to invert the signal.

The techniques used for the inversion of lidar signals, either from homogeneous or from inhomogeneous atmospheres, are discussed in sections 3.2 and 3.3. Parameters that effect the accuracy of the results are also discussed. Because the effects are easiest to understand in a homogeneous atmosphere most of this discussion appears in section 3.2. The results from the inhomogeneous atmosphere are also sensitive to these errors, but their effects can only be quantified when information on the shape of the profile is available.

3.2 Inversion of horizontally measured signals

Lidar signals from a homogeneous atmosphere, with $\alpha(R)=\alpha$ and $\beta(R)\beta=\beta$ in equation (3.1), are first corrected for the range term in the denominator. Taking the logarithm of the range compensated waveform yields:

$$\ln[S(R)] = \ln(K_1) + \ln(\beta) - 2\alpha R \quad (3.4)$$

The slope and the intercept of equation (3.4) are determined by linear regression which provides a direct measure for the extinction coefficient $(\alpha \pm \Delta\alpha)$ and the backscatter coefficient $\ln(\beta \pm \Delta\beta)$. This procedure is generally known as the 'slope method'.

The standard deviation in the extinction and the backscatter coefficients must be critically considered for the following reasons. In a very clear atmosphere, the signal is very weak and thus the range is limited. Moreover, the slope of the range compensated signal is very small. This may lead to unexpected large uncertainties in the calculated extinction- $(\alpha \pm \Delta\alpha)$ and backscatter coefficients $[\ln(\beta \pm \Delta\beta) = \ln(\beta) + \ln(1 + \Delta\beta/\beta)]$. On the other hand, if the extinction is large, the signal is strong but the range of the lidar signal (and thus the number of samples) is also limited due to attenuation. (A method to calculate the maximum range of a lidar system is presented in Appendix A.) Due to the limited number of samples, this can also lead to large uncertainties in the calculated extinction- and backscatter coefficients. In conclusion, the errors are smallest for intermediate extinctions. In Figure 3.1 the standard deviations in the extinction, $\Delta\alpha$, and in the backscatter, $(\Delta\beta)$, as inverted from the data base, are presented as a function of the extinction and the backscatter, respectively. As shown, the deviation of the largest extinction values (10 km^{-1}) is less than 1 km^{-1} (i.e. 10 %), while for the lowest extinction values (0.05 km^{-1}) they may amount to 10-100 %. Best results are obtained with this system for extinction coefficients around $0.5-1 \text{ km}^{-1}$.

which is about a factor of two larger than the extinction at which the maximum range is obtained. The standard deviation for the backscatter shows a minimum around 0.02 km^{-1} and increases with the backscatter. A more detailed analysis of the errors in the extinction- and backscatter coefficients determined by the slope method is presented in Kunz and DeLeeuw, 1992.

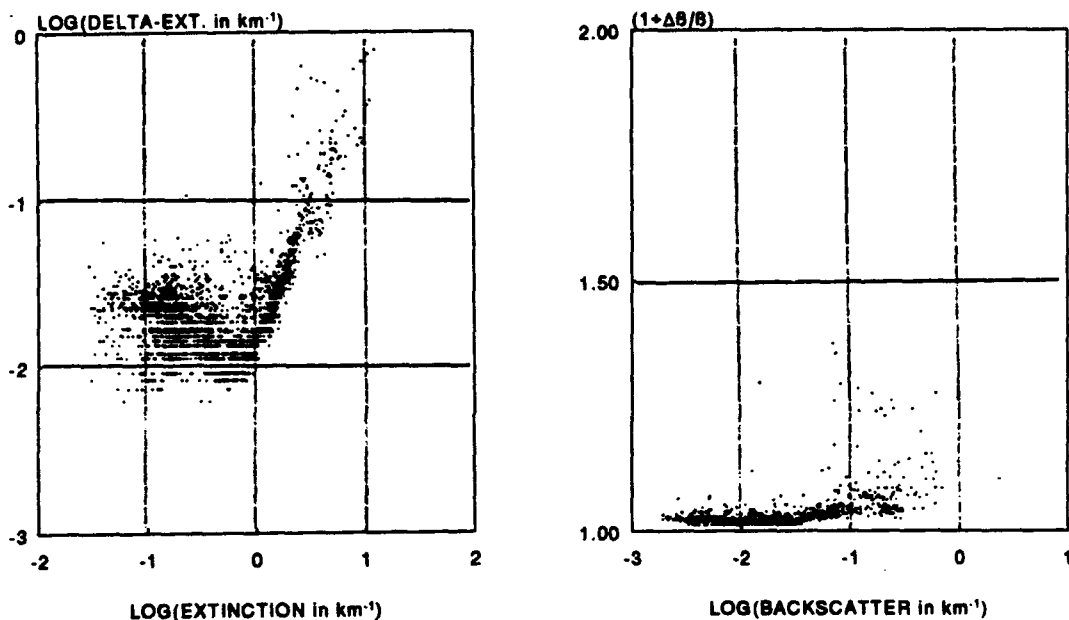


Figure 3.1: Deviation in the extinction coefficient and in the backscatter coefficient as a function of the values of the extinction and the backscatter coefficients, during the first months of 1985. The maximum range of the Mini-Lidar is about 1.3 km. This is reached when the extinction is about 0.4 km^{-1} and the backscatter is about 0.028 km^{-1} . See also Appendix A.

Although the slope method seems to be very simple, many effects can influence the final results. The resulting errors are not only dependent on the accuracy of the measurement, but also on the strength of the signal itself. Some sources of errors are:

- the trigger moment accuracy

Range compensation is the basic operation in lidar signal processing. However when the trigger moment is not accurately known, unintended compensation with $(R \pm \Delta R)^2$ is performed instead of with R^2 . This leads to errors in both the extinction and the backscatter coefficients. For example, an error of one sample interval of 30 ns introduces an error in the

extinction is 0.1 km^{-1} . The effects of the trigger moment accuracy are discussed in more detail in appendix C.

- the accuracy of the transfer of the log-amplifier

The transfer function of the logarithmic amplifier has two constants, L_1 and L_2 . The uncertainties in the constants influence both the backscatter and the extinction. The error is not only dependent on the error in the transfer but also on the strength of the signal. In particular, low extinction values are sensitive to uncertainties in the transfer of the log-amplifier. As explained in Appendix D, the uncertainty in the backscatter due to the transfer function is less than 3 %, but the error in the extinction varies from less than 2 %, for $\alpha = 1 \text{ km}^{-1}$, to more than 300 %, for $\alpha = 0.01 \text{ km}^{-1}$.

- the influence of the bandwidth

Bandwidth reduction has the advantage to improve the signal-to-noise ratio. However, the shape of the signal is distorted when the bandwidth reduction is beyond the frequency contents of the lidar signal. For example, signals with a short rise time, such as from a cloud return, are reduced in amplitude. Also signals from a homogeneous atmosphere are influenced. Although deconvolution can theoretically restore the original signal, experience shows that large errors remain in the final results. The amount of error introduced depends both on the strength of the signal and on the bandwidth of the filter. It is not simple to give a closed form expression for the error because the actual error depends also on the cross-over function of the lidar and on the initial condition of the filter. Simulations of homogeneous signals, with extinctions from 10^{-3} km^{-1} to 10 km^{-1} and with filter time constants between 10 and 1000 ns, show that a range of about $2.10^9 * \Gamma \text{ m}$ (Γ is the time constant in seconds of the first order filter) is required to eliminate the influence of the reduced bandwidth (Kunz, 1979).

- the accuracy of the reference level

Signals are temporarily stored in a transient recorder which must have the capability to store small negative signals as well (noise). This means that the signals are recorded with a small (numerical) offset which must be subtracted before the data are processed. When this subtraction is not done or not done accurately, large errors in the calculated results are possible. Also here, a closed form expression for the error is not possible because it depends on the system in question, the transfer of the electronics and the actual values of the

extinction- and the backscatter coefficients. This problem has also been indicated by Shimuzu (1985).

the resolution of the A/D converter

An inherent property of lidar signals is the large dynamic range which varies from 3 to 6 decades or more. To record these signals with sufficient accuracy, an A/D converter of 10 bits or more is required. When the VISA experiments were made (1985-1986) these instruments were very expensive, if available. Part of the problem has been solved by applying a logarithmic amplifier with a dynamic range in the order of 4.5 decades. It has been shown (Kunz, 1990) that a combination of a logarithmic amplifier and an eight bit A/D converter is comparable with a fourteen bits A/D converter. Most errors occur in small signals at large ranges.

3.3 Inversion of vertically measured signals

Inversion of the extinction profile from the measured data is possible with e.g. equation (3.5) which has been described by a number of authors e.g. Hitschfeld and Bordan (1954), Klett (1983) and Kunz (1983).

$$\alpha(R) = \frac{S(R)}{\frac{S(R)}{\alpha(R_o)} - 2 \cdot \int_{R_o}^R S(x) \cdot dx} \quad (3.5)$$

where $S(R)$ is the range-corrected signal as shown in (3.4)

As can be seen from (3.5), $\alpha(R)$ can only be inverted if both $S(R)$ and a boundary condition $\alpha(R_o)$ are available. Furthermore, the equation can be solved either by integrating from the far-end ($R < R_o$) or from near-by ($R > R_o$). The forward integrating method has the advantage that the necessary boundary condition, $\alpha(R_o)$, can be obtained with the lidar itself from a measurement in the horizontal direction (where the atmosphere is assumed to be homogeneous, hence the slope method can be applied to the measurement). However, this method has the disadvantage that a singularity may occur when the boundary condition is too large. The backward-integration method has the advantage that there will be no singularity in the solution because a real input

boundary of the extinction is always positive. However, a disadvantage of the backward-integration method is that the determination of the boundary value from the lidar signal itself is not accurate. For the inversion of lidar signals as described in this report, the forward integration method has been applied.

Other methods to measure the vertical extinction and backscatter profiles are described in Kunz, 1988 and in Kunz, 1990.

The effects described in the previous section also introduce errors in the extinction profile inverted from lidar measurements in an inhomogeneous atmosphere. However, because there are so many different profile shapes, it is not possible to even indicate the effect of possible errors or to describe a general trend. A detailed analysis is necessary for each type of profile.

4

DESCRIPTION OF THE DATA BASE

This chapter gives an overview of the active periods of the lidar system and the number of profiles recorded during VISA. The lidar data and the independently recorded meteo data were first validated and subsequently merged. The parameters recorded in the final data base are described in Appendix E.

Figure 4.1 shows a calendar of the years 1985 and 1986 in which the active days of the lidar are indicated. The lidar was not operated during holidays, weekends, field experiments, reconstruction activities, data conversion and maintenance of the equipment. The days for which both lidar and meteo data are available have been encircled in the calendar. As can be seen from Figure 4.1, winter and spring periods are emphasized as regards the number of measurements. Very few measurements are available in summer and no measurements at all in September.

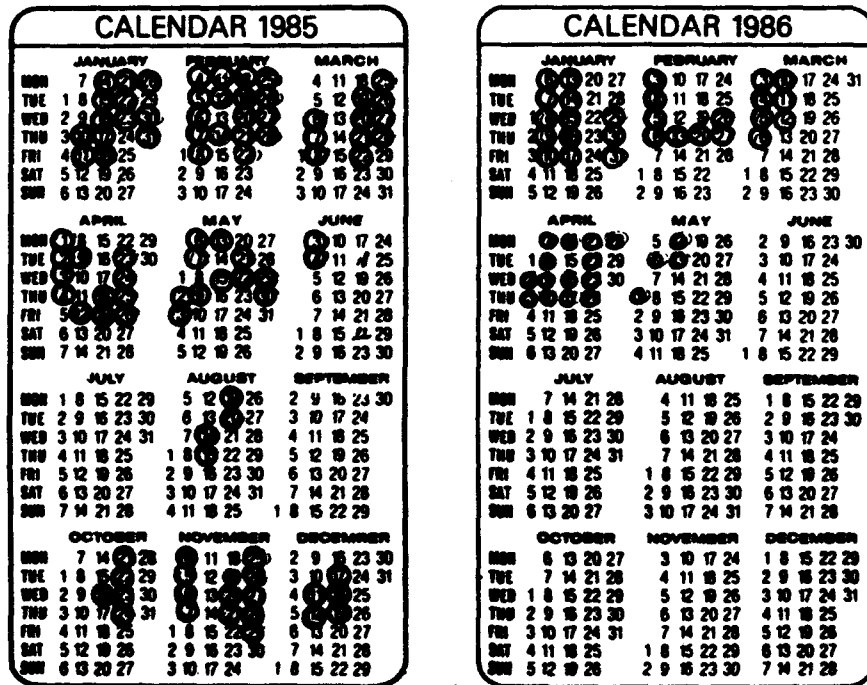


Figure 4.1: Calendar of 1985 and 1986, indicating the periods for which lidar data are available (gray) and for which combined lidar/meteo data are available (encircled).

The following table gives a numerical overview of the number of measurements:

year	lidar		meteo	
	files	records	files	records
1985	118	25,254	103	7,395
1986	71	12,231	64	5,110
total	189	37,485	167	12,505

Note: the meteo data was averaged every 15 minutes; the lidar measured a profile about every 7 minutes which causes the discrepancy between the number of lidar records and the number of meteo records.

After validation, merging and integration, the following number of files and records are available for analysis:

Combined files		
year	files	records
1985	91	15,869
1986	46	6,935
total	137	22,804

Analysis of the data base is described in the next section.

5 INVERTED DATA

Some typical examples of horizontal extinction- and backscatter coefficients, in relation with the actual meteorological condition, as well as some results of vertical atmospheric extinction profiles, are presented in this chapter. The altitude of the cloud base as measured during VISA has been described in Kunz, 1990.

5.1 Analysis of the horizontal measurements

For the inversion of lidar signals to vertical atmospheric extinction profiles, the horizontal extinction- and backscatter coefficients are necessary input parameters. They are also measured with the lidar. A logical sequence is therefore to concentrate on these parameters first.

- distribution of extinction and backscatter

Statistical overviews of the horizontal extinction- and backscatter coefficients are presented in Figure 5.1. All available records (22,804) were processed and distributed over 200 channels.

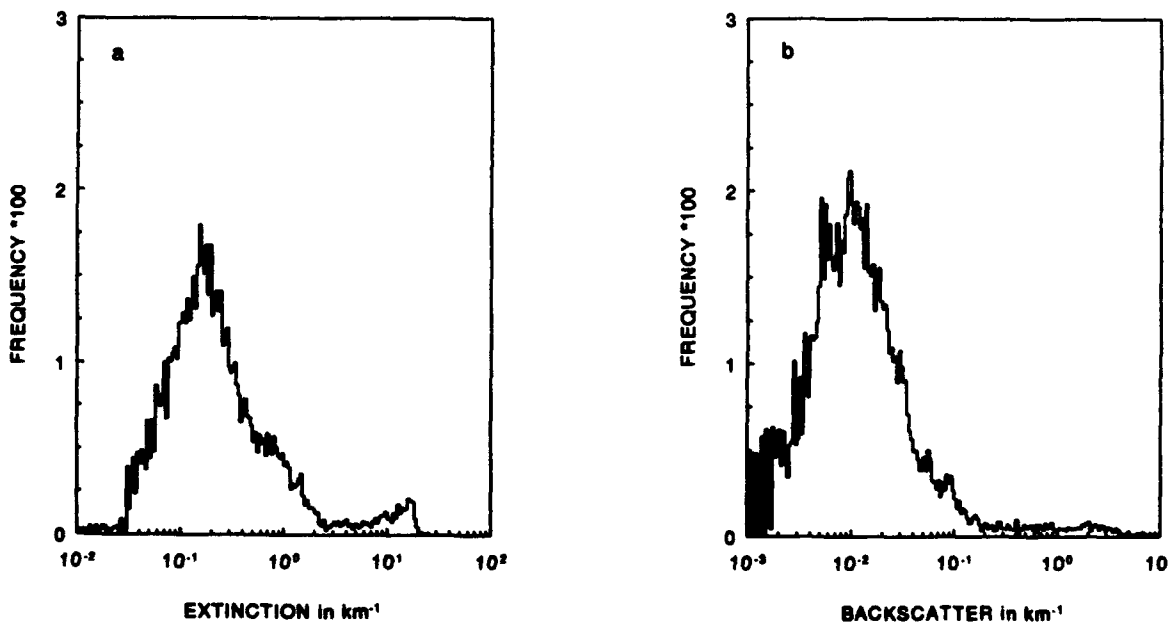


Figure 5.1: Frequency of occurrence of the 22,804 lidar measured horizontal extinction (a) and backscatter (b) coefficients

The histograms show that the maximum frequency of occurrence occurs at an extinction coefficient of about 0.16 km^{-1} and at a backscatter coefficient of about 0.01 km^{-1} .

- relation between extinction and backscatter (1)

For inversion of the vertical lidar measurements it is assumed that the ratio of backscatter and extinction (β/α) is constant throughout the mixed layer. Some authors even apply a fixed value. In our opinion this is not correct because the ratio depends on the aerosol properties which vary from day to day.

Three examples will be presented of periods were the ratio β/α :

- has a fixed high value
- has a fixed low value
- varies in time

An example of a period with fixed ratio β/α (but varying extinction and backscatter coefficients) is shown in Figure 5.2. In the period from 10:00 to 12:00 a.m., as indicated by '1', the measurements were performed in light snow resulting in enhanced β and α as well as a higher β/α ratio than in the period thereafter. In the period after 12:00 a.m., as indicated by '2', there was no precipitation.

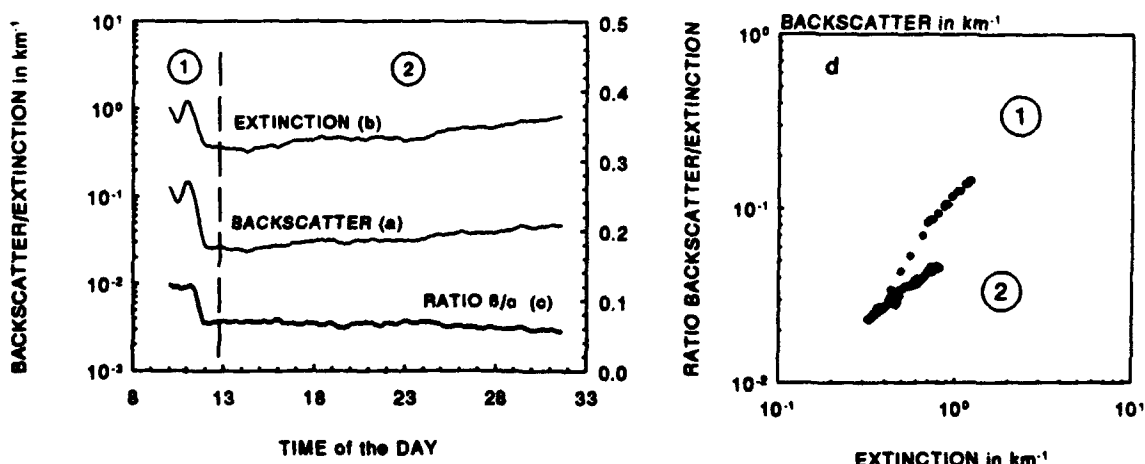


Figure 5.2: Left figure: Backscatter, extinction and ratio β/α on January 15-16, 1985 (time above 24 hours is the next day). From 10:00 a.m. to 12:00 a.m. it was snowing lightly. Right figure: scatter diagram showing the relation between extinction and backscatter.

The graphs in Figure 5.2 show that after 12:00 a.m. both the backscatter and the extinction varied by more than a factor 2, but the ratio β/α varied less than 10 %. Furthermore it can be seen that the ratio β/α in snow is larger than during the following period when there was no precipitation. The relation between β and α has also been visualized in a scatter diagram (Figure 5.2d). Another example of a period with a fixed but low value of the ratio β/α is shown in Figure 5.3. The period from 15:00 to 34:00 hours (i.e. 10:00 a.m. the next day), was characterized by a very good visibility (>40 km), in which β/α drops from 0.22 to less than 0.01. Although the backscatter and the extinction coefficients varied more than one order of magnitude during the whole day (see the scatter plots in Figure 5.3b), the ratio β/α varied about 20 %.

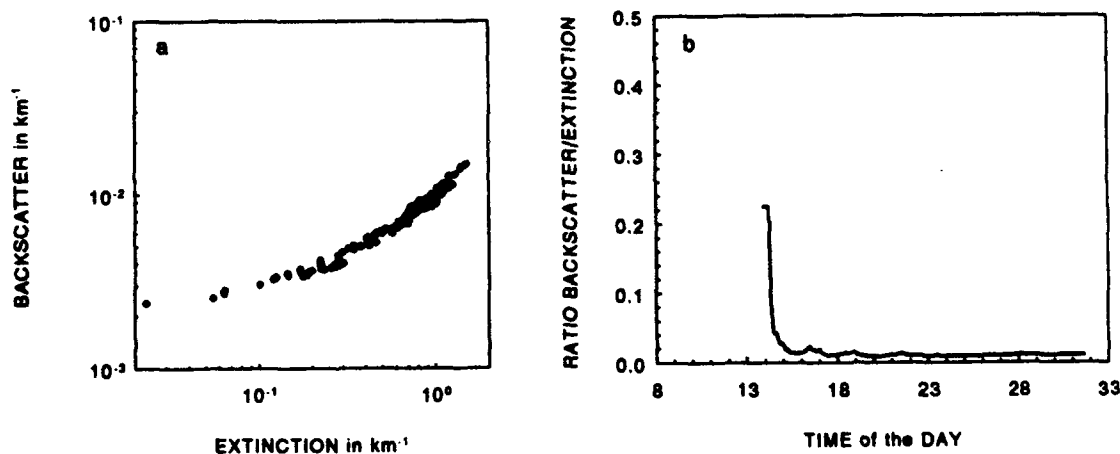


Figure 5.3: Scatter diagram of backscatter versus extinction (a) and the backscatter/extinction ratio as a function of time (b) on December 11, 1985 (time > 24 hours is the next day)

Figure 5.4 shows a period of a varying and slightly decreasing β/α ratio over a period of about 24 hours. From 11:00 a.m. to 07:00 p.m., the ratio β/α varies about 10 % and after 07:00 p.m., β/α decreases gradually from about 0.9 to about 0.6.

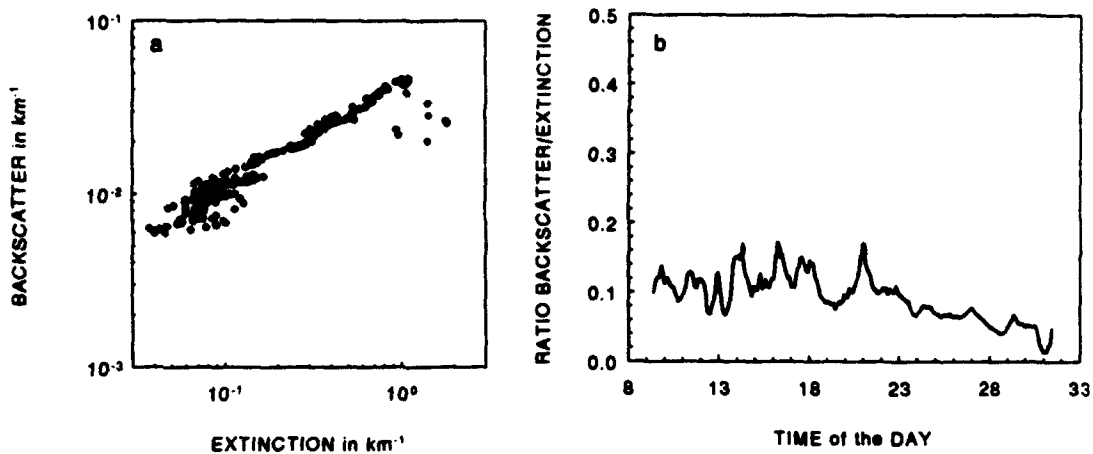


Figure 5.4: Scatter diagram of backscatter versus extinction (a) and the backscatter/extinction ratio as a function of time on January 30, 1986 (time > 24 hours is the next day). Temperature and visibility increased somewhat over the same period.

In the last example in this series, Figure 5.5, a period has been selected where both α , β and β/α vary strongly in time. The measurements were performed during a cloudless period with ground haze. The relative humidity varied from 60 %, before 06:00 p.m., to 90 % and more, after 07:00 p.m. (The variance in the backscatter is smaller than the variance in the extinction; not shown.) Compared to the previous examples, the variation in β/α is much stronger here.

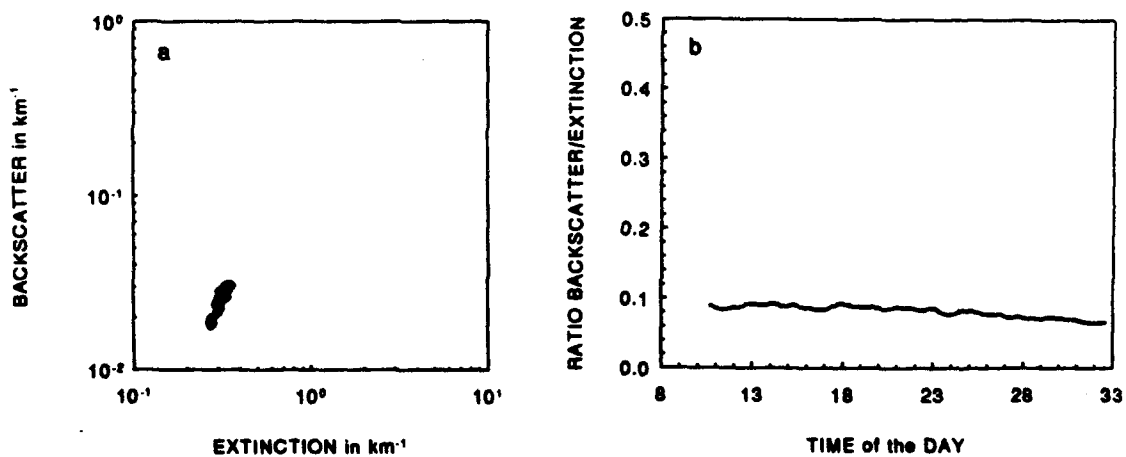


Figure 5.5: Scatter diagram of backscatter versus extinction (a) and the backscatter/extinction ratio as a function of time on February 5, 1985 (time > 24 hours is the next day). Temperature and visibility increased somewhat over the same period.

The selected results show that the ratio β/α in Figures 5.1, 5.3 and 5.4 are comparable. The low value of β/α in Figure 5.2 differs from the other examples. These results illustrate that the ratio β/α is not a fixed value but may vary from day to day and during a day.

- standard deviation in extinction and backscatter

The extinction- and the backscatter coefficients are calculated with the slope method from the log-range corrected signal (linear regression). During this process also the standard deviation of the extinction and of the backscatter are calculated. The standard deviations are not only caused by electronic noise but also by atmospheric structures (See also Kunz, 1992). It is expected, that due to the atmospheric structure the standard deviation decreases with the length of the selected interval (more samples) which, in turn, depends on the actual extinction (and backscatter) as explained in Appendix A. It is expected that the standard deviation reaches a minimum for a certain value of extinction (or backscatter). This effect has been observed in many data files. Figure 5.6 shows a typical example of this effect for both the extinction and the backscatter.

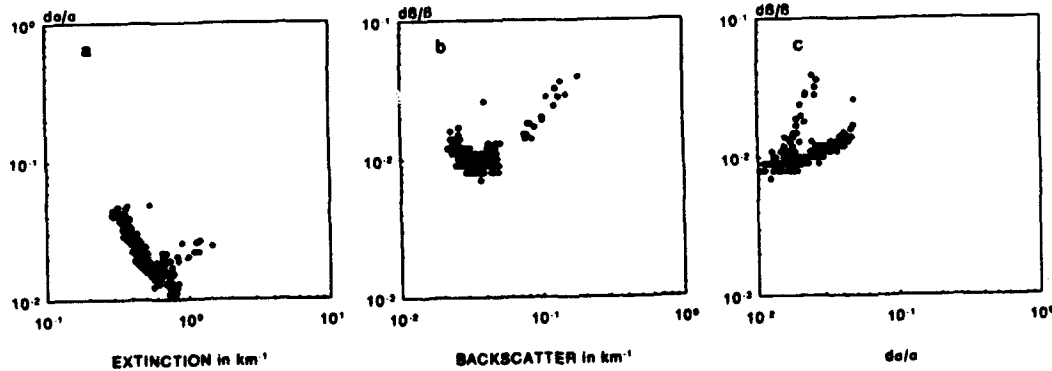


Figure 5.6: Scatter diagrams of the standard deviation of the extinction (a) and of the backscatter coefficients (b) as a function of the extinction and the backscatter. Scatter diagram (c) shows the relation between $d\beta/\beta$ and $d\sigma/\sigma$.

The analysis of many of the data files has shown that the relative deviation in extinction (or backscatter) has indeed a 'V' shape (See also Figure 3.1). Furthermore it appears that the minima of the variation in both the extinction and the backscatter occur almost simultaneously.

- relation between extinction and backscatter (2)

In the Figures 5.2 to 5.5 some daily periods were presented of the ratio β/α . The histograms for the extinction and the backscatter are presented in Figure 5.1. It is also interesting to review all the available data for the ratio β/α . However, presenting all available data in a scatter plot of β versus α yields one dark spot. Therefore the averaged β values and their standard deviations were calculated for discrete values of the extinction as shown in Figure 5.7. To this end, the extinction has been partitioned over 200 channels. The data were further separated into periods with and without precipitation. Results for the dry situation are shown in Figure 5.7b, those obtained during rain are presented in Figure 5.7c.

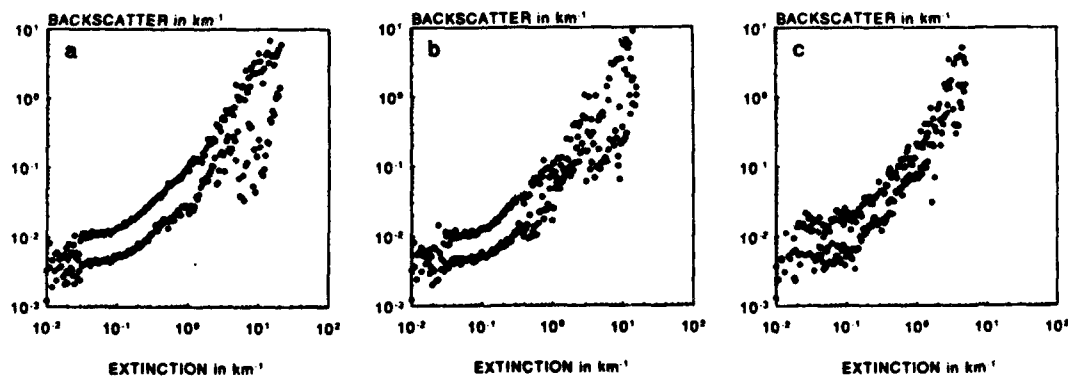


Figure 5.7: Relation between extinction- and backscatter coefficients for all data records (a), for situations without precipitation (b) and with precipitation (c). The upper and lower traces correspond with the mean backscatter plus or minus one standard deviation.

The results in Figure 5.7 indicate a non linear relation between β and α which becomes less evident for extinctions larger than about 5 km^{-1} . This is probably due to local fluctuations in α and β . For extinctions smaller than 0.03 km^{-1} , inaccurate determination of the extinction causes the variability of β/α , see Kunz and DeLeeuw, 1992. In that case the backscatter can be

determined more reliably than the extinction. Precipitation has only been recorded during working hours because no instrument was available at that time for automatic indication. It is clear from Figure 5.7 that there is no distinct difference in the overall shape of the three figures. This means that (this) lidar provides similar results both in dry weather and during precipitation. For low values of the extinction and the backscatter, the backscatter seems to reach a limiting value of about 0.004 km^{-1} which is about a factor 3 larger than the Rayleigh backscatter value ($1.3 \times 10^{-3} \text{ km}^{-1}$). For extinctions larger than about 5 km^{-1} , a second mode becomes visible in which the backscatter is about one order of magnitude lower. A more detailed analysis shows that this is only present in a few files; thus far, the reason for this behaviour is not understood.

- relation between relative humidity and extinction or backscatter

The relation between the relative humidity and the backscatter, the extinction and the ratio β/α is an other subject of interest (e.g. DeLeeuw et al, 1986 and Tonna, 1991) because the relative humidity tends to increase with height in the atmospheric boundary layer. It is generally assumed that there is a positive correlation between the relative humidity and the extinction, the backscatter and/or the backscatter/extinction ratio. From a review of all the data files, it appears that the correlation between the relative humidity and the backscatter is better than the correlation between the relative humidity and the extinction. The relation between backscatter and relative humidity has in many cases been observed to loop back during a period of rising and falling relative humidity (cf. Figure 5.10). This may be caused by the anomalous growth of hygroscopic aerosol which has been reported e.g., by Winkler, 1971.

Some typical examples of the relation between the lidar measured extinction- and backscatter coefficients and the relative humidity, are shown in the Figures 5.8 to 5.10. Figure 5.8 shows the scatter plots of the extinction and the backscatter coefficients versus relative humidity, as recorded over a 24-hour period. These plots illustrate that the variation in the extinction at $\text{RH} > 90\%$ is larger than the variation in the backscatter. The backscatter increases slightly when the relative humidity increases from 54 % to 90 %. For higher values of the relative humidity, the backscatter increases much stronger. This effect has been observed in many data files. However, we noted that the relation between backscatter and relative humidity varies from day to day.

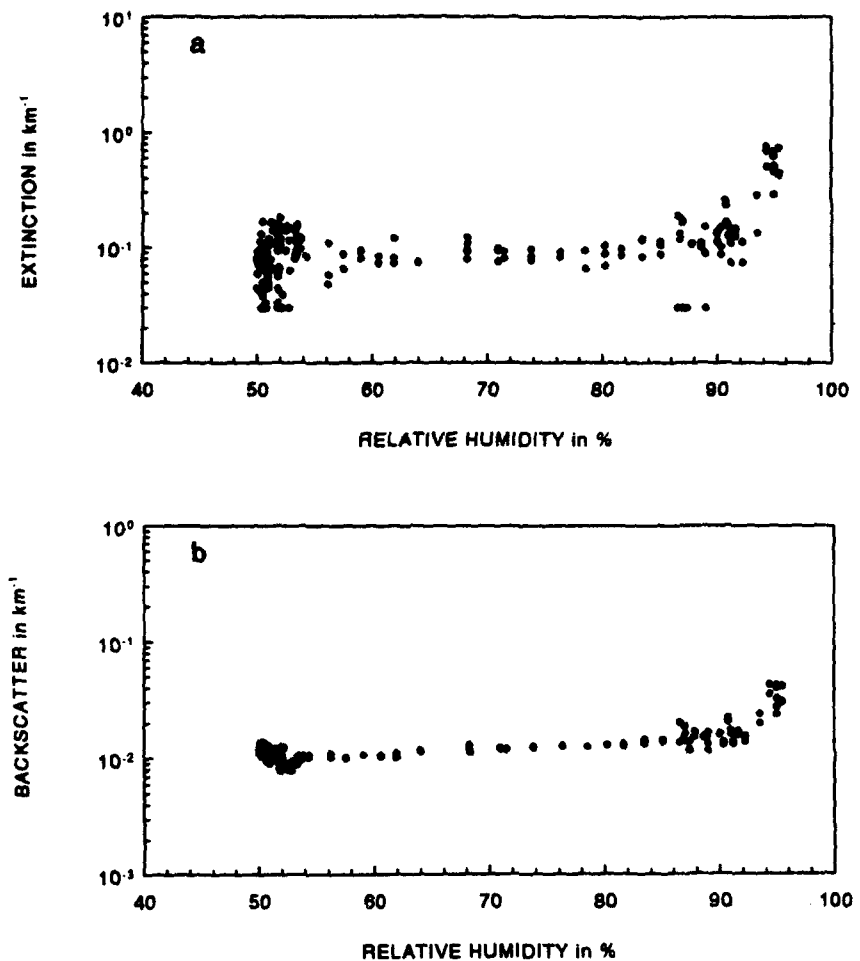


Figure 5.8: Scatter diagram of the extinction versus relative humidity (a) over a period of 24 hours on February 20, 1985 and the scatter diagram of the backscatter and the relative humidity (b). Note that the variation in the backscatter is smaller than the variation in the extinction.

Figure 5.9 shows another scatter diagram of the backscatter versus the relative humidity, recorded on March 26, 1985 when higher values of the relative humidity occurred. The measurement period was about 24 hours. For values of the relative humidity smaller than 97 %, the backscatter varied by a factor of about 2, but for higher relative humidities the variations were up to three orders of magnitude. It is noted that accurate relative humidity measurements near 100 % are extremely difficult. Therefore, results from routine measurements should be carefully interpreted in this regime. When the recorded relative humidity approaches 100 %, this might correspond to a situation where the relative humidity goes slightly over 100 % (due to inherent instrument inaccuracy) and aerosols can be activated. The activated aerosols grow in size very fast, resulting in a strong increase in both the extinction- and backscatter coefficients.

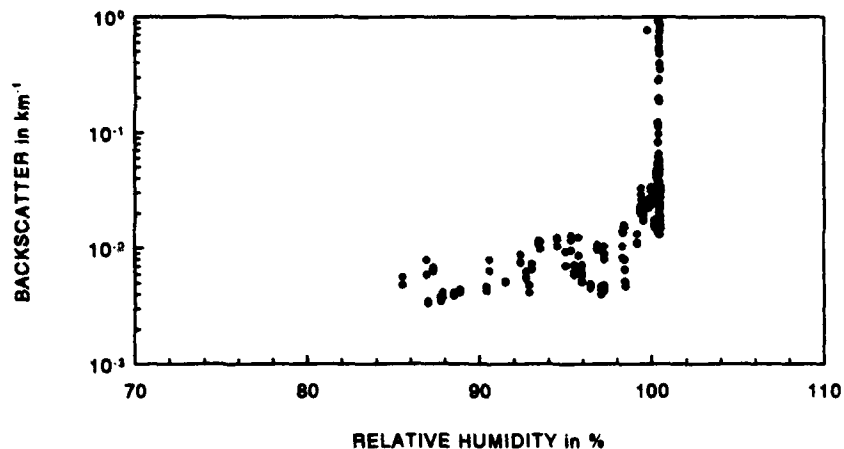


Figure 5.9: Relation between backscatter and relative humidity, for high values of the RH, over a period of 24 hours on March 26, 1985. For $\text{RH} < 90\%$ there is a positive correlation; for higher values of the RH there is no relation at all.

Figure 5.10 shows an example where variations in the relative humidity result in a 'hysteresis loop' in the backscatter. This behaviour has been observed many times.

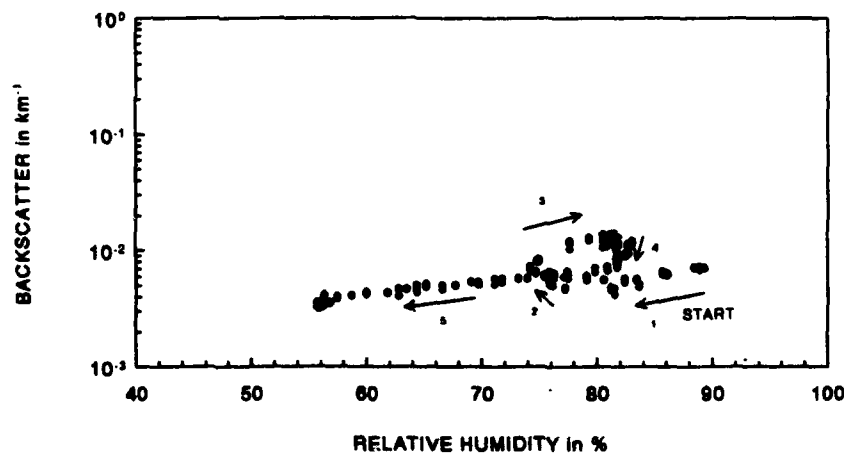


Figure 5.10: Relation between the backscatter and the relative humidity over a period of 24 hours on February 7, 1985. Note the curl between 74 and 82 % relative humidity.

- relation between visibility and extinction or backscatter

The visibility, the backscatter and the extinction coefficients are an evident set of parameters which should correlate. Results of this kind have been published and discussed in the past (among others, by Lamberts, 1978, Lamberts and DeLeeuw, 1986 and Bertolotti, 1969, 1978). Some of the relations derived from our data set will be presented below.

In Figure 5.11 an example is shown of a 24 hour period where both the extinction and the backscatter coefficients are well correlated with the visibility. For high visibilities, the deviation in the extinction is larger than the deviation in the backscatter.

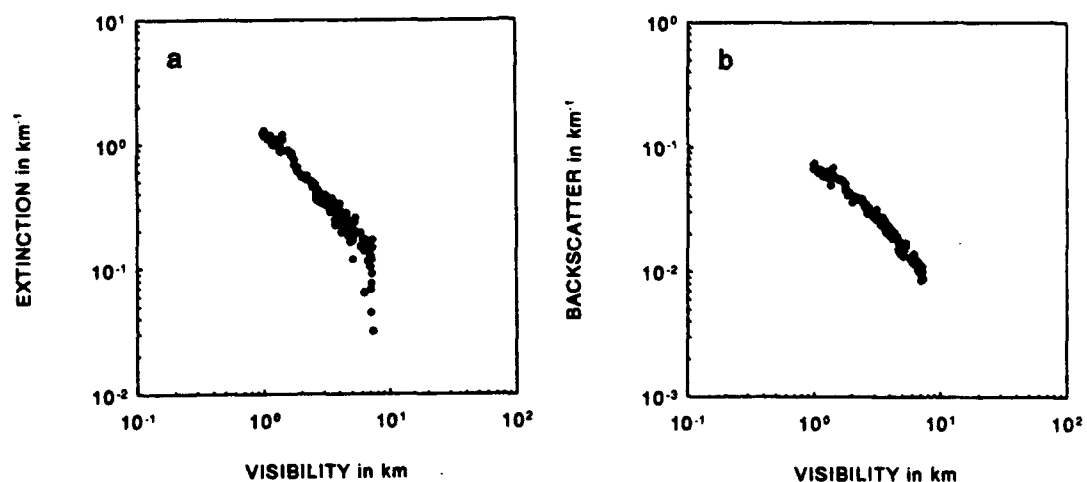


Figure 5.11: Scatter diagram of the extinction coefficient (a) and of the backscatter coefficient (b) as a function of the visibility over a period of 24 hours on March 10, 1986 (time above 24 hours is the next day). Note that both the extinction and the backscatter correlate well with the visibility.

Analysis of all validated data files shows that the relation between visibility and backscatter or between visibility and extinction is not always as good as shown in Figure 5.11. In many cases, the visibility correlates either better with the backscatter or with the extinction. In other cases no correlation at all is found. Figure 5.12 shows an example where the visibility correlates better with the extinction (range interval from about $0.5-2 \text{ km}^{-1}$) than with the backscatter. In Figure 5.13, however, where the extinction varies from about $0.03-1.5 \text{ km}^{-1}$, the visibility correlates better with the backscatter.

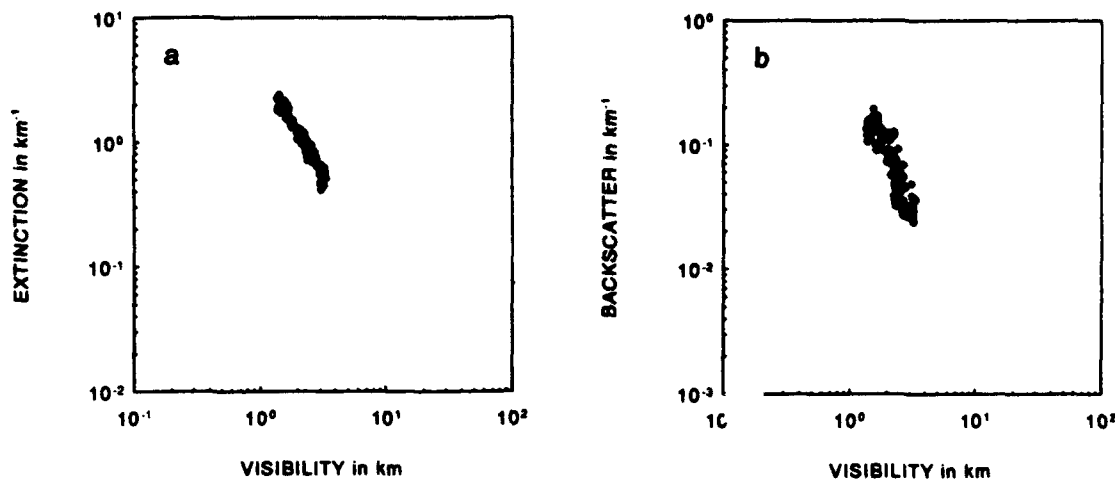


Figure 5.12: Scatter diagram of the extinction (a) and the backscatter (b) as a function of the visibility measured over a 24 hour period on April 7, 1986. Note that the correlation between extinction and visibility is better than the correlation between backscatter and visibility.

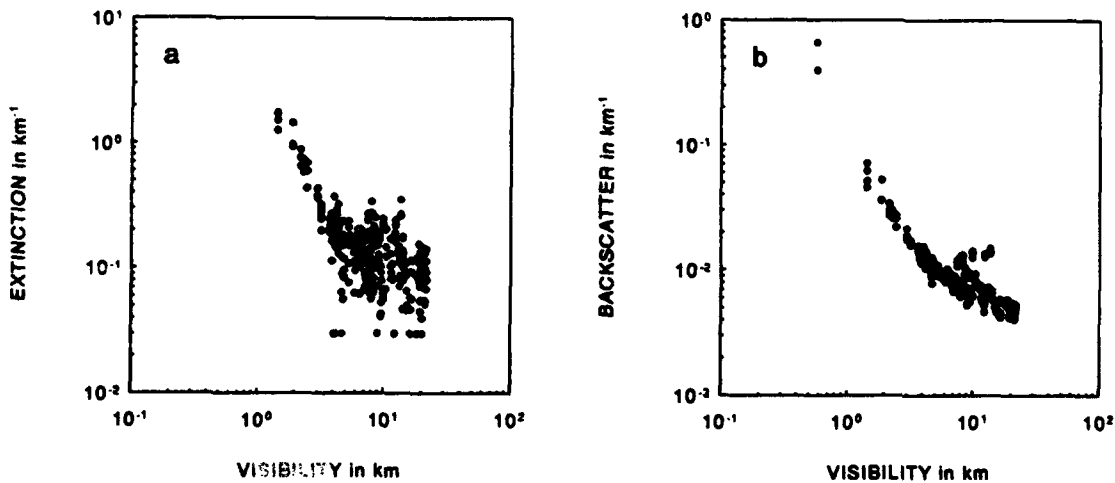


Figure 5.13: Scatter diagram of the extinction (a) and the backscatter (b) as a function of the visibility measured over a 24 hour period on April 18, 1986. Note that the correlation between the backscatter and the visibility is better than the correlation between the extinction and the visibility.

The last example in this series shows that there are also periods where neither the backscatter nor the extinction correlate well with the visibility. This is shown in Figure 5.14.

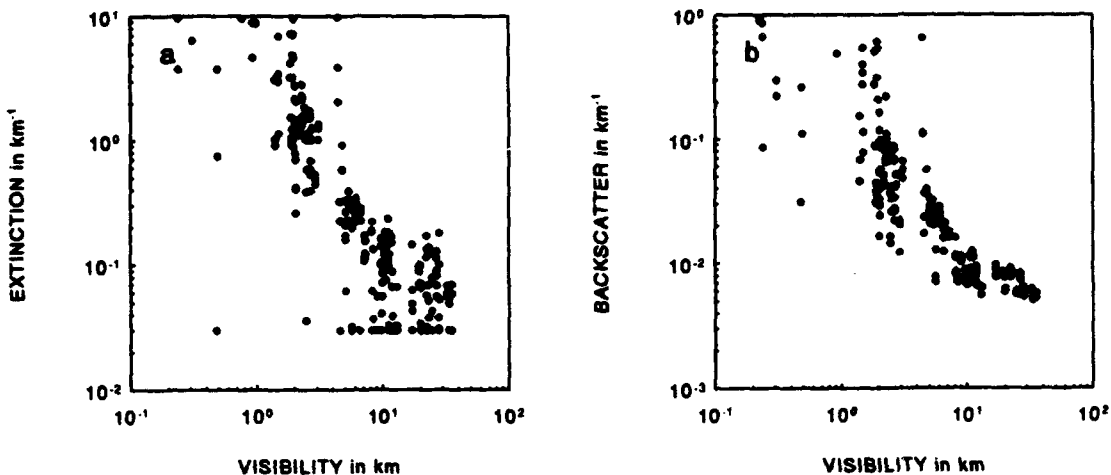


Figure 5.14: Scatter diagram of the extinction (a) and the backscatter (b) as a function of the visibility measured over a 24 hour period on February 21, 1986. Example of a poor correlation between the visibility and the scattering coefficients.

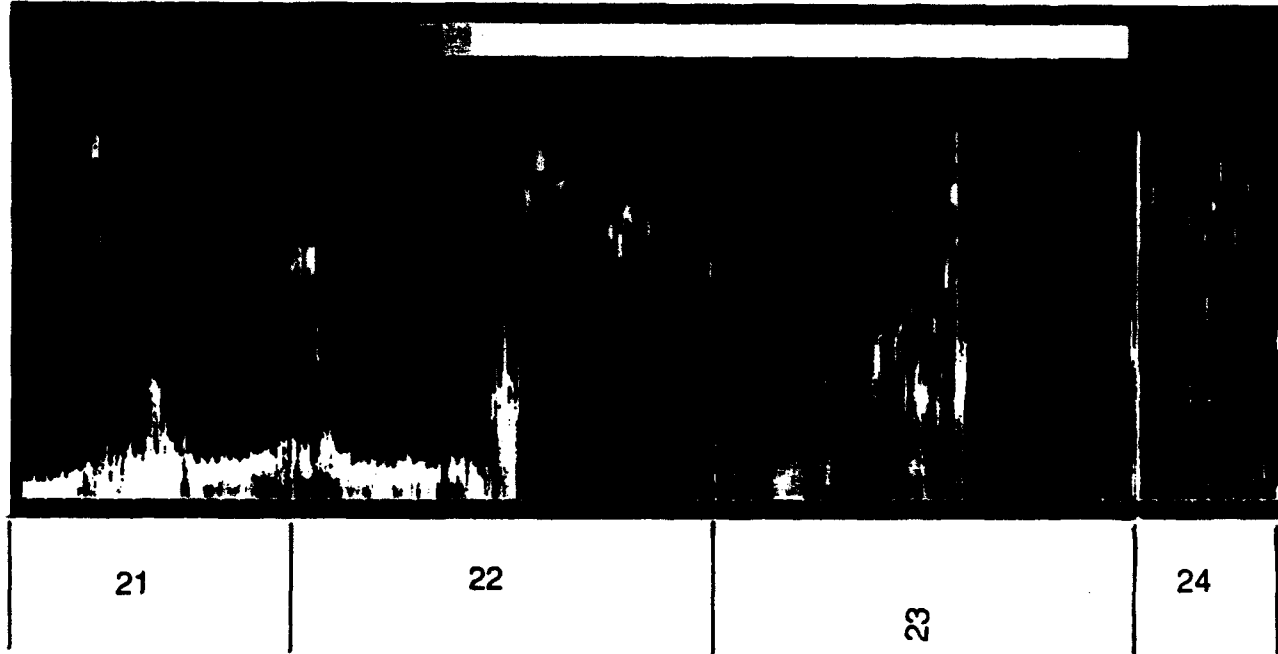
5.2 Analysis of vertical measurements

Knowledge of the vertical structure of the atmosphere is of importance for many disciplines. Especially processes in the atmospheric boundary layer (up to 1-2 km) play an important role for human life. These include both observable processes, like haze and wind, and the transport of pollution, mixing of air from different altitudes, etc. The vertical or slant path visibility is an important parameter in avionics; the altitude and behaviour of the mixed layer are also important for meteorology.

Results from measurements of vertical atmospheric extinction profiles during the VISA project are presented for selected periods. As far as possible, examples are presented of profiles which were measured during several days to one week in each month of the year, to give an impression of possible seasonal effects. Results are presented as false color plots, where the altitude is plotted along the vertical axis and the time is plotted along the horizontal axis. The extinction, which is the third parameter in these figures, is coded in false color. The color scale is plotted on top of each figure for reference. Hourly intervals are indicated by thin vertical ticks at the top and the bottom while the days are separated by white vertical lines.

- result of January 1985

Vertical extinction profiles, as measured in the period January 21-24, 1985, are presented in Figure 5.15. An external mirror was used to reach a maximum altitude of 2000 m. The measurements were performed after a period of snow and ice, when the thaw set in.



January 1985

Figure 5.15: Vertical extinction profiles coded in false color from January 21 (8 a.m.) to January 24 (8 a.m.), 1985. The maximum altitude was 2000 m.

On Monday January 21, 1985, from 08:21 a.m. to about 11:30 a.m., the extinction profiles could only be measured to an altitude of about 80 m due to a ground fog. The extinction coefficient was very high (about 2 km^{-1}). Between 11:30 a.m. and 04:00 p.m., the extinction at ground level decreased and profiles could be measured up to an altitude of about 1400 m. Then a cloud layer descended from about 500 m to about 200 m at 07:00 p.m. Subsequently the cloud layer rose gradually to about 300 m and the extinction at ground level decreased correspondingly to about 0.2 km^{-1} . After midnight, a new cloud layer was detected at about 1200 m. A low-altitude cloud base, decreasing from about 300 m altitude to about 200 m altitude, was present until about 11:00 a.m. on January 22. At that moment, a cloud layer was detected at about 500 m altitude during about two hours; the wind velocity decreased from about 8 m/s to about 4 m/s. This cloud layer

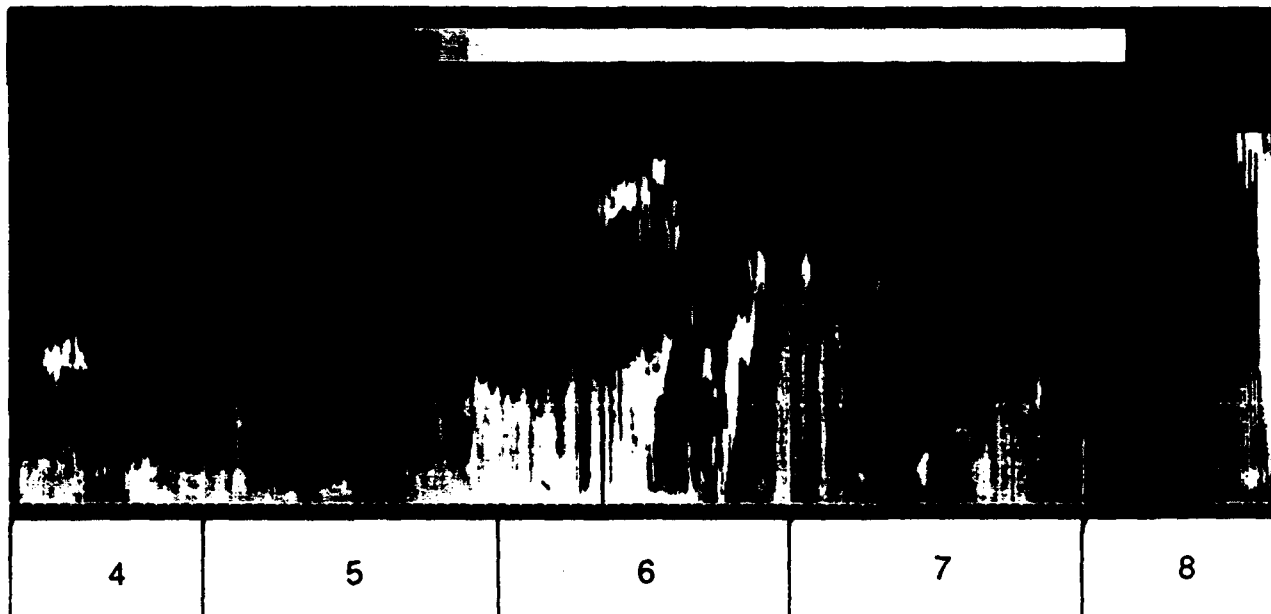
suddenly disappeared after 01:00 p.m. but other cloud reflections were observed at altitudes between about 1400 m and 1600 m. Periods with clear skies occurred during the night (human observation), accompanied by relatively low extinction values at ground level. After mid-night, the extinction at ground level increased until about 05:00 a.m. on January 23. Between 09:00 a.m. and 02:00 p.m. the cloud base varied between 500 and 1500 m altitude. Starting around noon this day, patches of clouds were detected at different altitudes during the afternoon, evening and night. The wind was strong. On January 24 the behaviour was similar to that observed during the night before.

Discussion:

The results from Figure 5.15 show the dissolution of the ground haze in the morning of January 21 and the increase in the depth of the mixed layer. The altitude of the cloud layers, which are indicated by small white vertical lines or small white patches, was very instable and varied between 80 m and 2000 m during this period. Note that the influence of clouds below 500 m altitude is perceptible in the extinction some hundred meters below the cloud base.

- example of February 1985

Figure 5.16 shows extinction profiles to an altitude of 2000 m over a period of 5 consecutive days. The measurements started on February 4, at 08:43 a.m. and ended on February 8, at 03:28 p.m.



February 1985

Figure 5.16: Vertical extinction profiles coded in false color in a height versus time plot. Period: February 4, 08:43 a.m. to February 8, 1985, 03:28 p.m.

At the beginning of this period, some ground haze was present. In the log was recorded that the sky was covered with thin cirrus (not visible in the figure). Starting at 11:00 a.m., a layer with increased extinction was detected at 750 m altitude. This was probably not a cloud layer because there was also sunshine during this period. The extinction at ground level decreased. At 05:00 p.m., the depth of the mixed layer started to decrease from about 750 m altitude to about 200 m at 08:00 a.m. on February 5. (This resulted in a ground haze, the extinction at ground level increased until about 07:00 p.m.) This ground haze stayed during the night and morning (observed visually). During the night the sky was clear and there was some frost. After 08:00 a.m. on February 5, the mixed layer rose gradually to about 700 m altitude, which was reached around 10:00 p.m. The extinction increased and clouds were visually observed (not shown in the figure). Although the altitude of the mixed layer was constant during the night and the morning on February 6, the top of the mixed layer showed a strong convolving behaviour with a period of almost two hours. The extinction at ground level increased significantly resulting in a misty morning. Between around 07:00 a.m. and 08:00 a.m., the height of the fog layer extended to about 100 m altitude. From

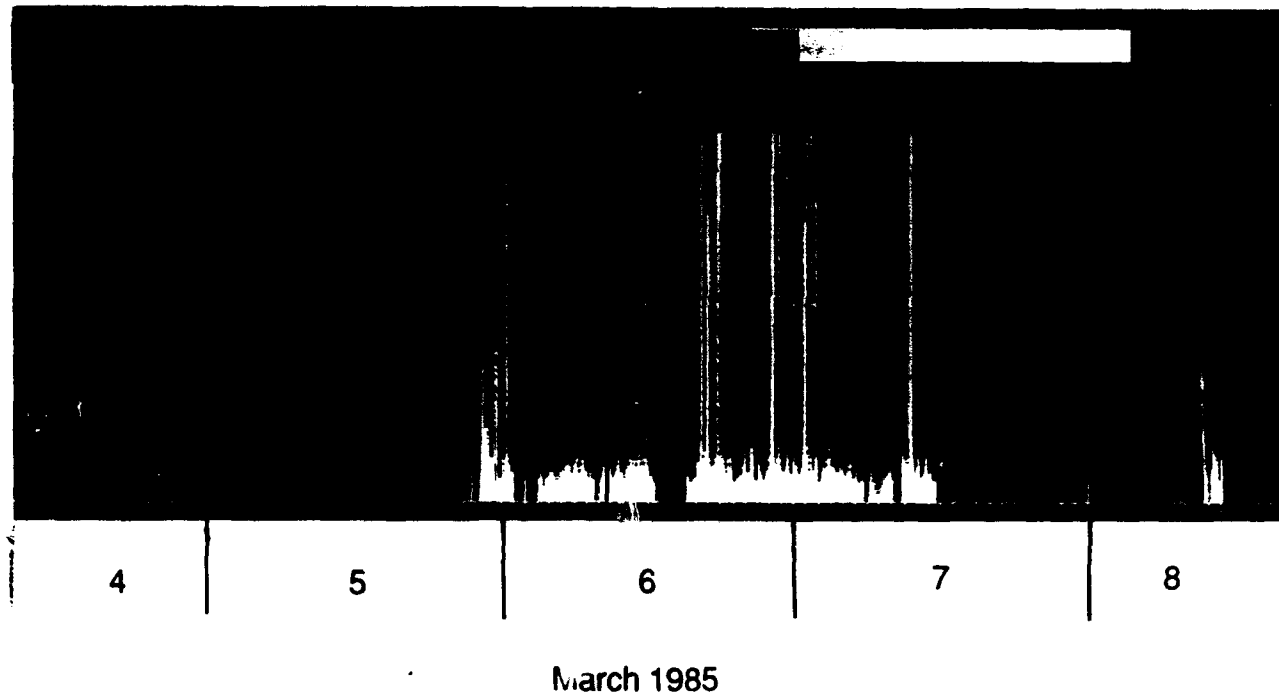
08:00 a.m. to 03:00 p.m. on February 6, a cloud layer was detected at about 1500 m altitude. Around 01:00 p.m., the fog layer appeared to separate into a ground fog layer and a cloud rising from about 400 m to about 1000 m altitude. From 06:00 p.m. to about 10:00 p.m., a cloud layer is detected which rose from about 100 m to about 1300 m altitude. During the night, the depth of the mixed layer extended to about 1300 m altitude while a slight variation in extinction was visible; temperature decreased below the freezing point. On February 7, between 06:00 and 07:00 a.m., the height of the mixed layer decreased rapidly from 1000 m to 100 m. After 08:00 a.m. the mixed layer rose gradually from about 100 m to about 800 m at 09:00 p.m. During the night and the morning on February 8, the height of the mixed layer varied somewhat around 500 m altitude while the extinction itself decreased gradually to a minimum around 07:00 a.m.. After 00:30 p.m., a rapidly descending cloud layer was detected.

Discussion

The morning warming effect is clearly visible on February 5, 7 and 8 starting at about 09:00 a.m.. The effect of increasing extinction during the night is visible on February 4 and 5 and partly on February 7. The depth of the mixed layer varied from less than 100 m to more than 2 km and is the average depth was about 700 m. The meandering effect of the top of the mixed layer is clearly visible in the night from February 5 to 6 and in the morning of February 6.

- example of March 1985

Figure 5.17 shows an example of extinction profiles, coded in false color, as measured with lidar during five consecutive days from March 4, 08:45 a.m., to March 8, 03:30 p.m.



March 1985

Figure 5.17: Vertical extinction profiles, coded in false color, from March 4-8, 1985. The period from 8:30 a.m. to 02:30 p.m. on March 4, was characterized by rain showers. The strong extinction during March 6 and 7 was caused by a ground haze.

The period from 08:30 a.m. to 02:30 p.m., on March 4, was dominated by many rain showers. The cloud base was detected around 200 m. After 02:30 p.m., the cloud base rose to about 900 m. After 04:30 a.m., the clouds vanished and the sun appeared. During the clear night, the temperature at ground level decreased below 0° C and ground haze was formed. The height of the mixed layer remained below 250 m altitude. The extinction started to increase at about 10:00 p.m. on March 4 until 08:00 a.m. on March 5. At about 08:00 a.m., the ground haze dissolved and disappeared completely at 01:00 p.m. From that time on, the extinction at ground level increased strongly and reached its maximum value at midnight. The depth of the mixed layer remained almost constant at an altitude of about 100 m. At 01:00 p.m. on March 6, the ground haze disappeared and the sun was visible during about two hours. This was followed by an early morning ground haze which lasted until about 11:30 a.m. on March 7. (The high extinction values are not real but are caused by singularities in the forward inversion method.) During the night from March 6 to 7, the sky was clear. On March 7 at 11:30 a.m., the mixed layer deepened until

about 04:00 p.m. From that time to about 09:00 a.m. on March 8, the depth of the mixed layer meandered over an interval of about 50 m around an altitude of about 100 m. At 09:00 a.m. a cloud was detected and short thereafter a new ground haze formed.

Discussion

During the March period, there was much ground fog with a thickness of about 100 m. Diurnal effects were visible in the night from March 4 to 5 and during the morning of March 7. Several times, the forward inversion method failed in the ground fog (March 5 from 10:00 p.m. to March 7 at 11:00 a.m.). During modest fog (March 7, 06:00 to 08:00 a.m.) the vertical atmospheric extinction profiles could be measured and inverted. This can be seen from the structure at larger altitudes. On March 7, the mixed layer rose with a velocity of about 50 m per hour.

example of April results

The results of the vertical extinction profiles measured from April 15 to April 19, 1985, are shown in Figure 5.18. This dry period was characterized by a clear sky and ground haze. On April 15 at 08:50 a.m., the measurements started under a cloudy sky with a cloud base at about 500 m. After 09:00 a.m., the extinction in the mixed layer decreased until about 11:00 p.m. At 01:00 a.m. on April 16, a cloud was detected at about 250 m and the extinction at ground level increased rapidly. At 06:00 a.m., a new cloud layer was detected at about 700 m altitude which remained there until about 08:00 p.m. Note that the extinction below the cloud started to increase already at an altitude of about 300 m. Between 05:00 p.m. and 07:00 p.m., a haze layer was observed to move in from the sea. This resulted in an increase in the extinction between 200 and 600 m altitude. During the night from April 16 to April 17, a ground haze developed. The depth of this layer decreased slowly. Minimum altitude was reached between 03:00 and 04:00 a.m. From that time on, the top of the ground fog layer ascended from about 100 m to about 250 m. A second layer was detected which rose from about 200 m to 550 m altitude. From 01:00 to 03:00 p.m., the atmosphere above 100 m was clear. At about 04:00 p.m., cumulus clouds were observed and at 05:00 p.m. a new ground fog layer developed which stayed until 01:00 p.m. on April 18. At that time the extinction decreased due to deepening of the mixed layer. From about 04:00 p.m. on April 18 to about 02:00 a.m. on April 19 the thickness of the mixed layer decreased. Subsequently a new layer was detected at an altitude of about 700 m which descended slowly until 10:00 a.m. to an altitude of about 100 m. From that time on this layer ascended and dissolved.

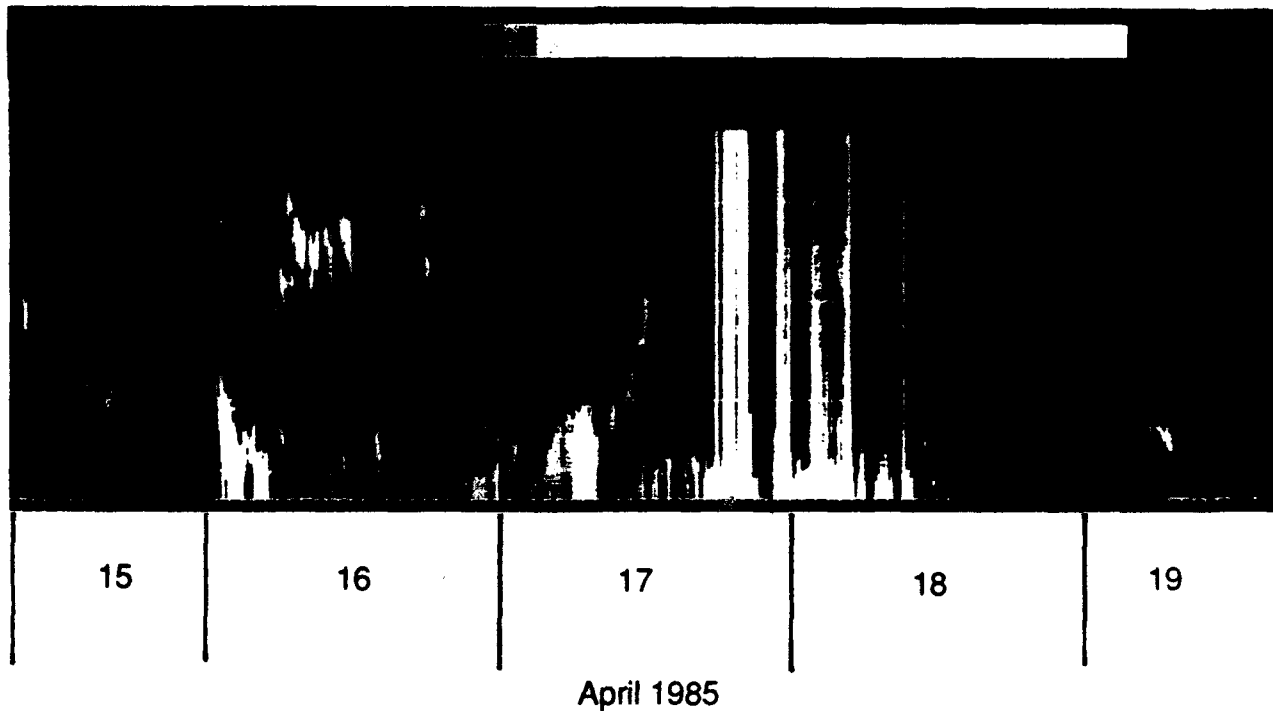


Figure 5.18: Vertical extinction profiles, coded in false color, in the period April 15 to 19, 1985; maximum altitude 1000 m. The mixed layer varied in altitude from about 400 m to more than 1000 m altitude. No precipitation was observed during this period. Ground haze was present from April 16, 02:00 a.m. to April 18, 12:00 a.m.

Discussion:

The April period showed a mixed layer with a varying thickness from about 200 m to more than 1000 m. The appearance and dissolution of fog layers were clearly mapped. In part of the period, the inversion of some lidar returns failed due to the very strong extinction at ground level. During two days, a rise of the mixed layer in the morning has been observed. The rate was about 120 m per hour. The data from figure 5.18 also show that the extinction underneath a cloud can extend over several hundreds of meters.

- example in May 1985

Results of vertical atmospheric extinction profiles as measured with lidar in the precipitation-free period on May 6-10, 1985 are shown in figure 5.19. The measurements started on May 6, 1985 at 09:23 a.m. The log reported that cirrus clouds covered the sky and that some ground haze was present which stayed until about 03:00 p.m. The thickness of the mixed layer grew while the extinction at the surface remained unchanged. Also when the sun came through, the surface

extinction did not decrease. During the evening and the night (including the morning of May 7) the ground extinction increased and reached maxima around 02:00 a.m. and 08:00 a.m.. At 08:00 a.m., the sky was fully overcast (which is not visible in the lidar results). From 09:00 a.m. to 03:00 p.m. the height of the mixed layer decreased somewhat and after 03:00 p.m. it increased again. The extinction at ground level also increased and reached a maximum at about 10:00 p.m. Subsequently the ground extinction varied somewhat and reached a new maximum at 06:00 a.m. on May 8. At about 07:30 a.m. the altitude of the mixed layer started to rise, reaching its maximum at about 04:00 p.m., while the ground extinction decreased. Then a cloud layer was detected at about 1000 m altitude, which disappeared again at 08:00 p.m. From that time the ground haze, with a thickness of about 100 m, was detected and lasted for the rest of the period. From about 10:00 p.m. on May 8 to 09:00 a.m. on May 9, the surface haze layer was capped by a clear layer. On May 9 at 09:00 a.m. the sky was clear with sun shine. After 09:00 a.m. a new ground haze developed and this layer rose with a velocity of about 100 m per hour. The fog was also present during May 10 which resulted in a limited range of the lidar.

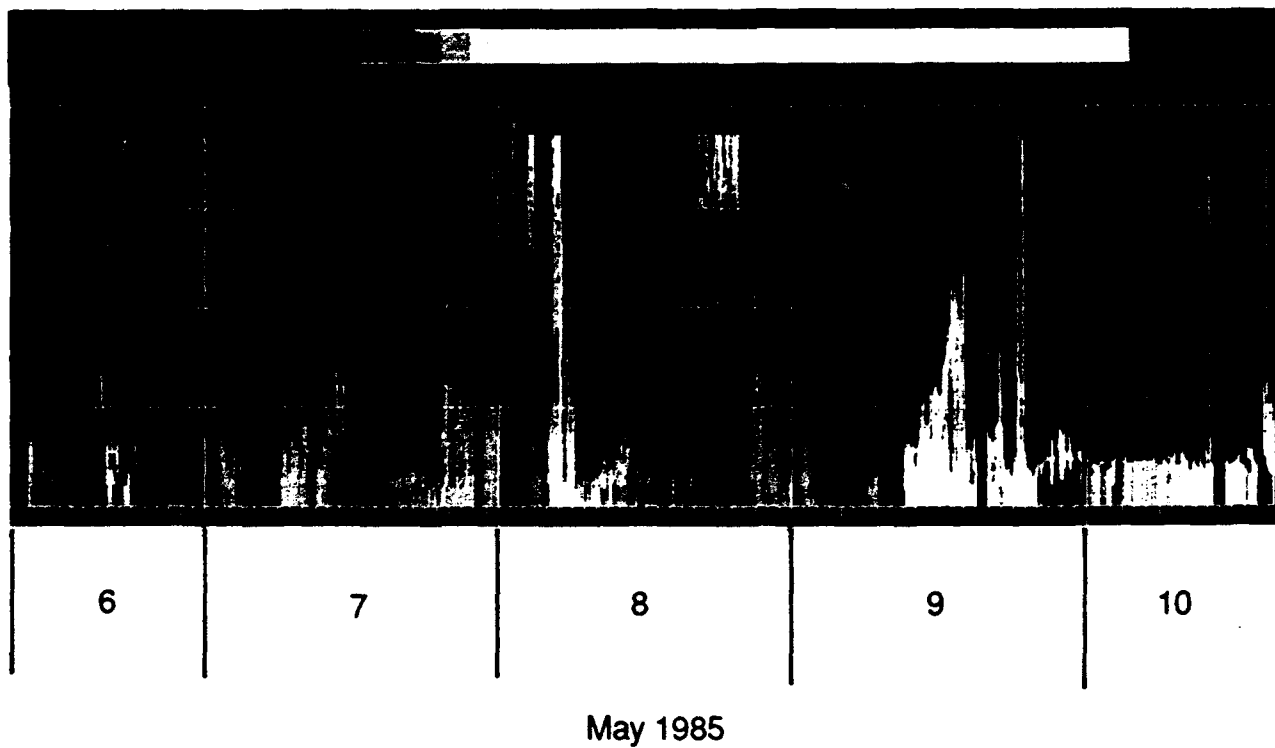


Figure 5.19: Vertical extinction profiles, coded in false colour, in a time versus height (0-1000 m) plot. Period from May 6 to May 10, 1985. The period is characterized with intervals of mist and haze but without precipitation.

Discussion:

Diurnal variations are visible on May 6, 7, 8 and 9. On May 7, 8 and 9, the development of ground haze has been observed with different extinction values.

- result of July/August 1985

The vertical atmospheric extinction profiles measured during the period July 29 to August 2, 1985, are presented in figure 5.20. During July 31 the sky was fully overcast without precipitation. The height of the cloud base varied from 500 m to over 1000 m but the cloud layer could not be distinguished clearly. During the night on July 29 and 31, ground mist layers were detected which reached altitudes of respectively 250 and 500 m. A diurnal effect is visible in the morning and in the evening of July 31.

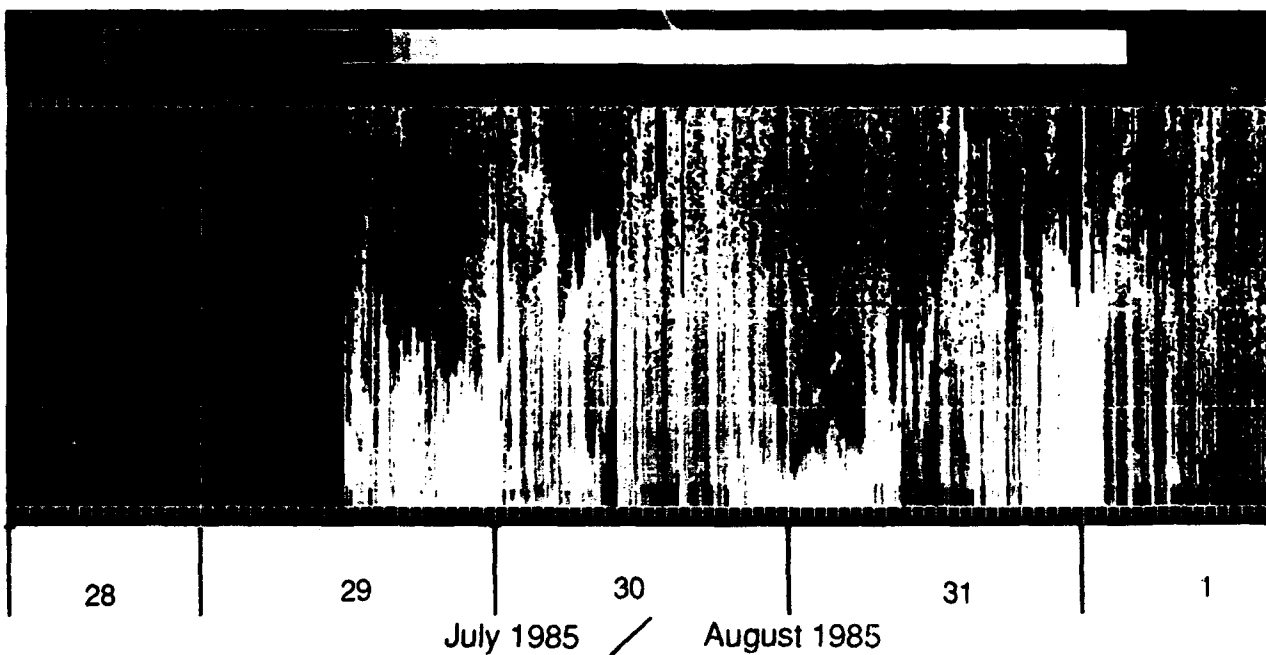


Figure 5.20: Vertical extinction profiles coded in false color, in a height versus time plot, measured with lidar in the period July 29 to August 2, 1986.

- example of October 1985

The vertical atmospheric extinction profiles measured during the fourth week in October 1985, are presented in Figure 5.21. No clouds were detected in this period. During the first three days, the height of the mixed layer varied between about 300 m and about 600 m. In the last two days, the depth of the mixed layer was about 250-350 m. During the night from 21 to 22 October and in the early morning of October 22, the depth of the mixed layer decreased to about 300 m and the extinction at ground level increased. Around 09:00 a.m., the height of the mixed layer rose again to about 600 m with a velocity of about 40 m/hour and the extinction at ground level decreased. At about 07:00 p.m., the mixed layer remained at a constant level of about 600 m until at least midnight on October 23. (Due to a system error, the lidar was not in operation from midnight October 23 until about 09:00 a.m. that day.) After 06:00 p.m. on October 23, the height of the mixed layer decreased significantly with a rate of about 80 m/hour. The extinction at ground level also decreased and reached a minimum value at midnight. Note that this is opposite to the behaviour during the night from October 21 to 22. During the morning of October 24, the extinction at low altitudes increased until about 08:00 a.m. The minimum value of the extinction occurred at about 03:00 p.m. and increased gradually until October 25, 09:00 a.m. At that time, the height of the mixed layer started to rise.

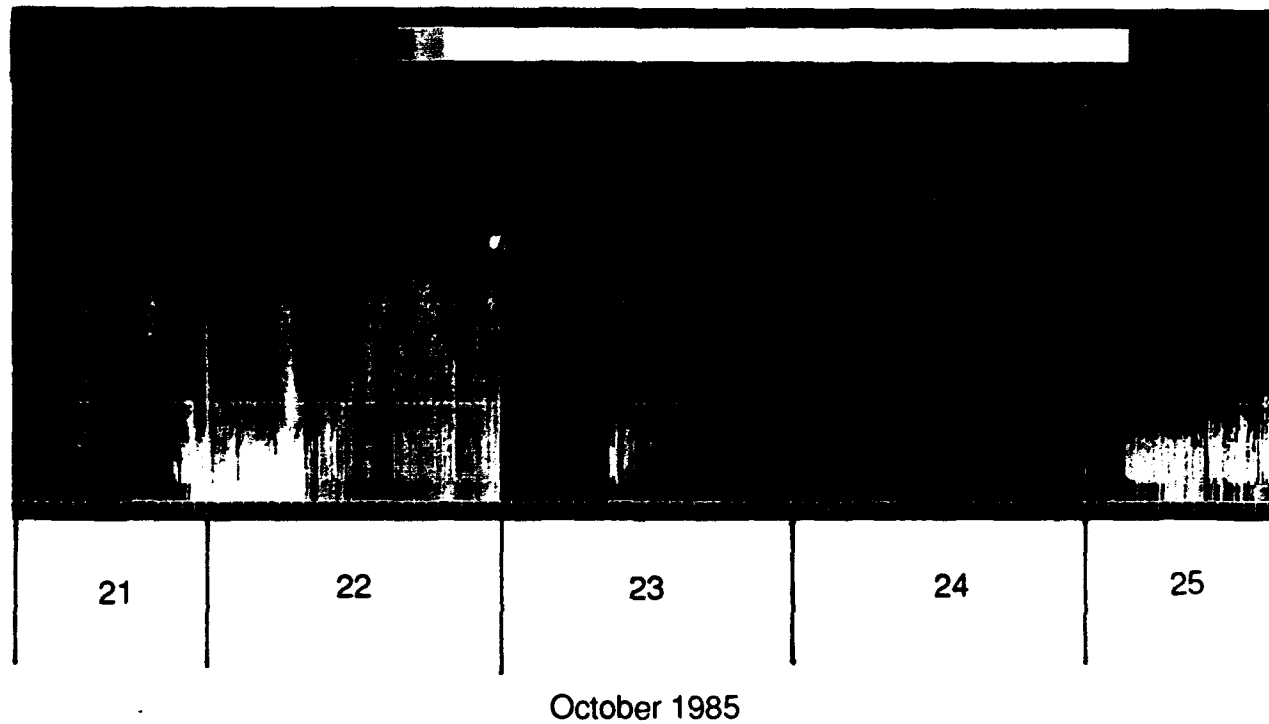


Figure 5.21: Vertical extinction profiles, coded in false colour, in a time versus height diagram. Period October 21 to October 25, 1985. Varying mixed layers, both in altitude and in extinction can be distinguished.

Discussion:

The vertical extinction profiles measured in the October period clearly show the process of a developing mixed layer with increasing extinction at low altitudes from midnight until about 09:00 a.m.

- example of November data

A series of vertical atmospheric extinction measurements in November 1985 is presented in Figure 5.22.

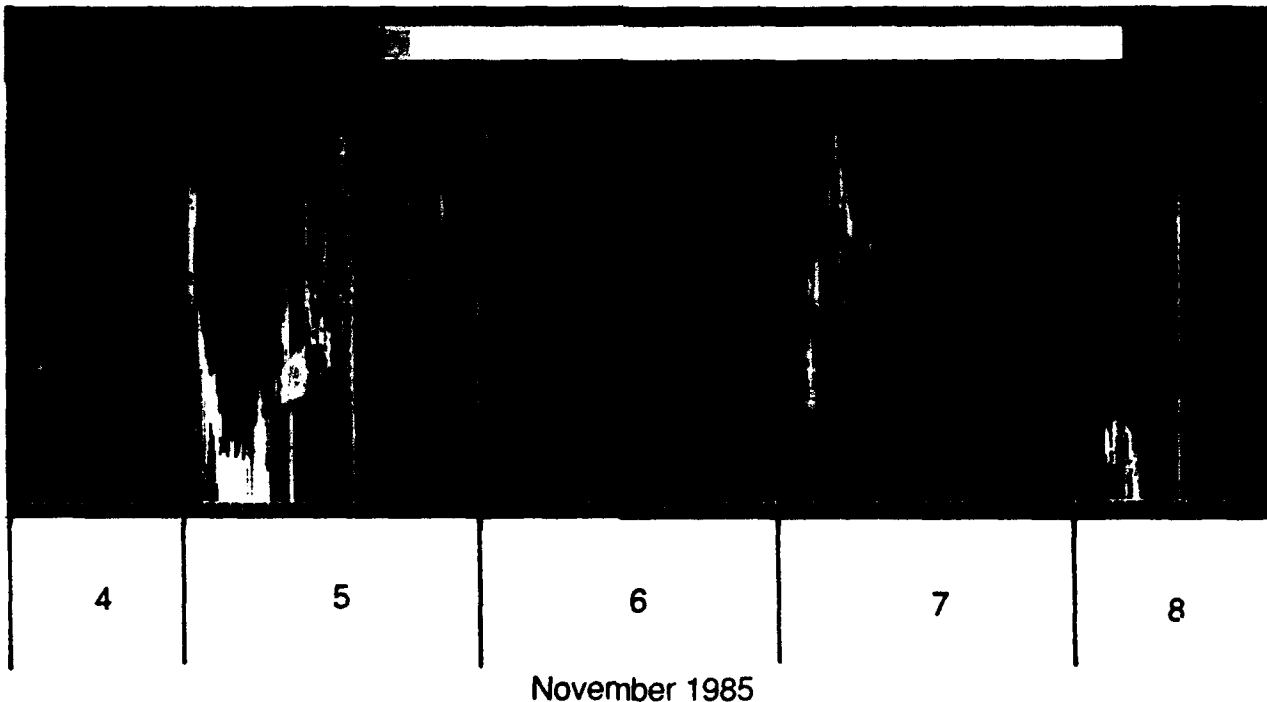


Figure 5.22: Vertical extinction profiles, coded in false colour, in a time versus height diagram. Period November 4 to November 8, 1985.

On November 4, the log reported that the sky was fully overcast, but the cloud reflections are not visible in Figure 5.22. (i.e. Cloud base was higher than 1000 m.) During the early morning on November 5 the cloud layer descended rapidly with a rate of about 150 m/hour and a fog layer with a thickness of about 200 m developed which remained until about 07:00 a.m. Diurnal effects are slightly visible in the extinction at low altitudes in the evening of November 4 and in the morning of November 7 and 8.

Discussion:

This November period is marked by relatively low extinction values at ground level (except in the morning of 5 November) and a variable extinction both in altitude and in time. Clouds were detected at different altitudes at irregular moments. The mixed layer varied between about 250 m and 1000 m and more.

General discussion

False color presentation of the vertical extinction profiles is a suitable method to present large amounts of (lidar) data in a quasi three dimensional figure. Although the figures give a qualitative impression of the temporal and spatial behaviour, the extinction values are quantitatively available. By reviewing the data files, it is noted that in contrast to what is generally assumed, the increase in the depth of the mixed layer during the morning is not always clearly visible in the measured data. This is also the case for the descend of the mixed layer in the evening and night. The reason for this might be the fact that many fronts with varying wind direction and different air mass (with different α and β) influence the atmospheric conditions in the Netherlands (See e.g. Lamberts and DeLeeuw, 1986). Furthermore, turbulent mixing due to solar heating was in many cases reduced by the presence of clouds. If present, the ascend rate of the top of the boundary layer is on the order of 100 meter per hour, as derived from the figures presented. Variations in altitude of the mixed layer have clearly been mapped with the lidar. The height of the mixed layer varies generally slowly (over hours), but also sudden changes on time scales of some minutes (including abnormal conditions like rain) have been observed. From the available measurements, it is possible to determine the path integrated extinction both in vertical sense as well in slant path.

5.3 Statistical review of the vertical extinction

The frequency of occurrence and the cumulative distributions of the extinction at altitudes of 15, 140, 265, 390, 525, 640, 765, 890 and 1015 m above ground level have been determined. This is at intervals of 125 m plus the altitude of the system at 15 m. To skip anomalies, only profiles in periods without precipitation have been included in this analysis.

- combined results from 1985 and 1986

The histograms of the extinction at the above mentioned altitudes, derived from all the 1985 and 1986 data files, are shown in Figure 5.23. The cumulative distributions are shown in Figure 5.24. The mean value and the standard deviation, both derived from the cumulative distribution and plotted as a function of height, are presented in Figure 5.25. The value of 0.2 km^{-1} , at 15 m altitude, is equal to the results of Figure 5.1 (frequency distribution of the horizontal extinction). The high frequency of occurrence in the figure at 15 m and 140 m are due to the choice of a boundary condition in those situations were the horizontal measurement did not provide an adequate solution.

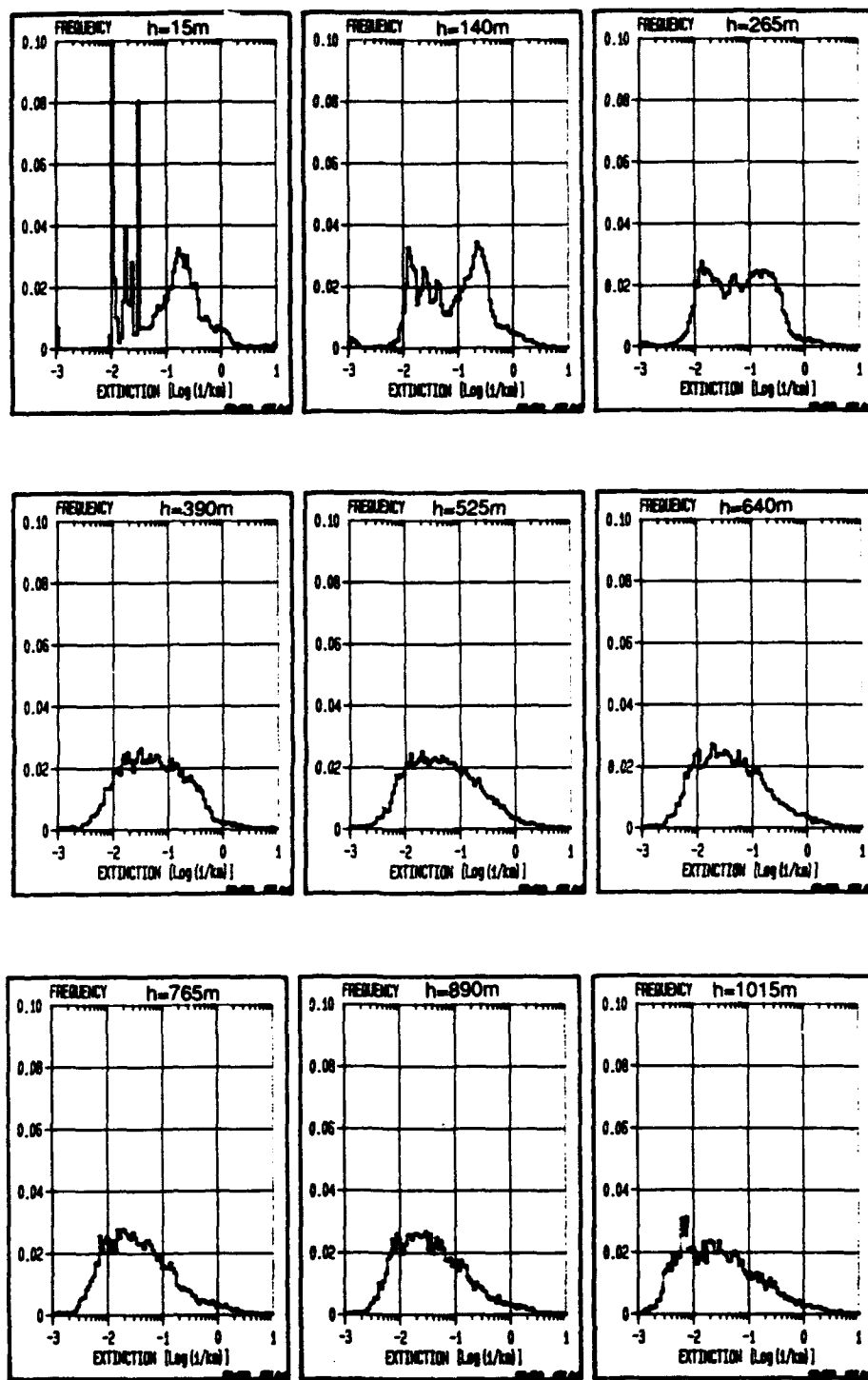


Figure 5.23: Frequency distribution of the atmospheric extinction at 9 different altitudes as derived from 11,000 lidar profiles.

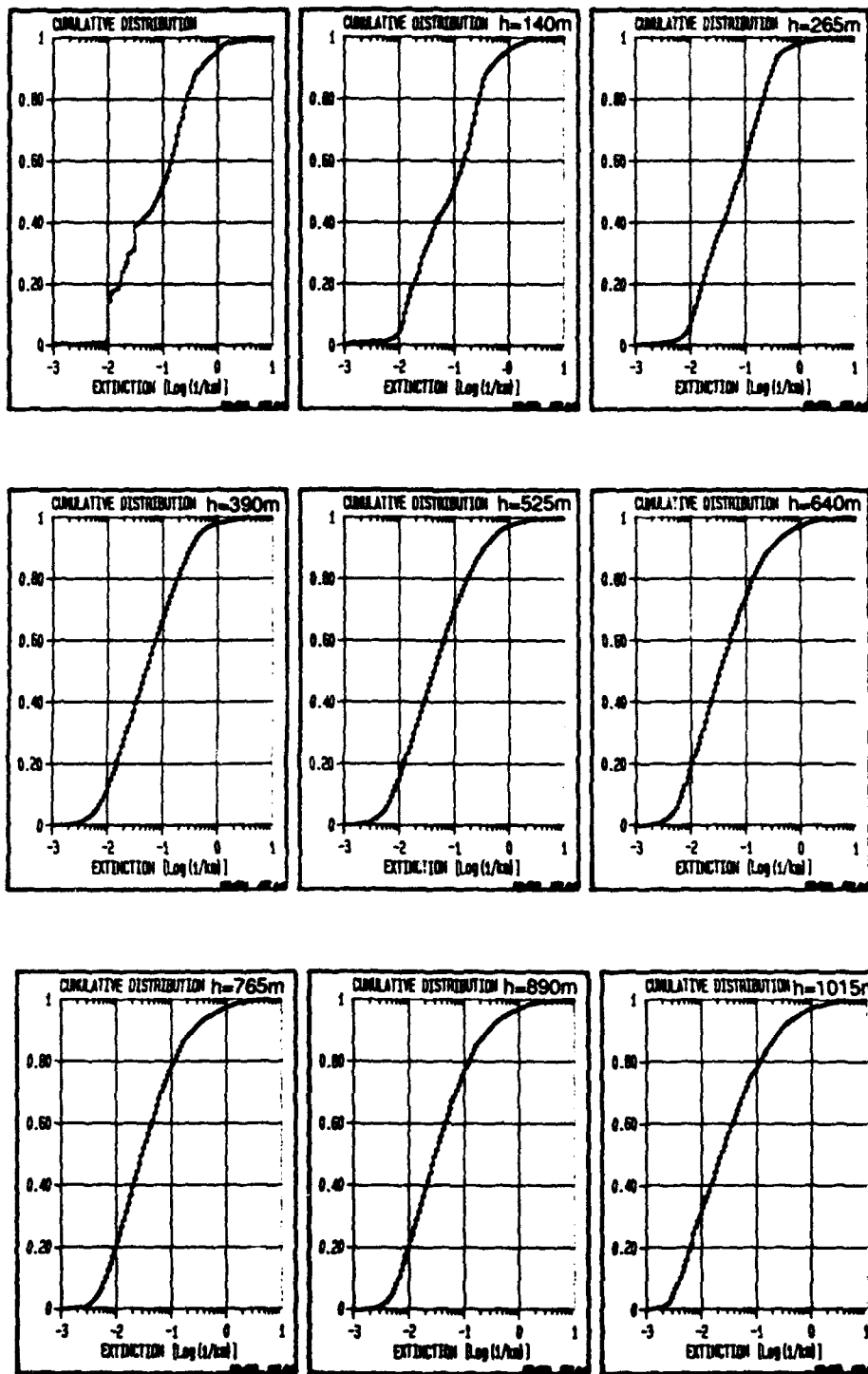


Figure 5.24: Cumulative distributions of the extinction at nine different altitudes. See also figure 5.23

The histograms in Figure 5.23 have different shapes at altitudes below and above 400 m. Below this altitude, a multimode behaviour is observed; above this altitude, the frequency distributions approach a skew Poisson distribution with a maximum likelihood at about 0.02 km^{-1} . The widths of the distributions are more than 1.5 decades. Very large extinctions (above 1 km^{-1}) are rare. The histograms at 390 m and higher shift gradually to somewhat lower extinction values. This means that there is a slight tendency that the extinction decreases as the altitude increases. This effect is better visible in Figure 5.25.

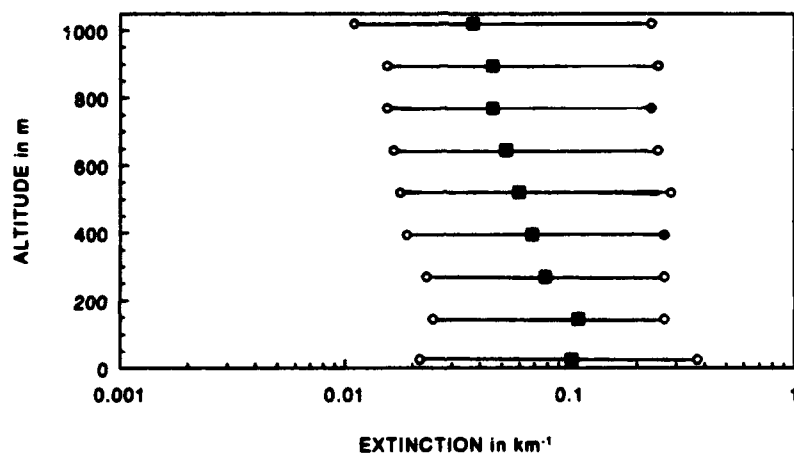


Figure 5.25: Mean (solid squares) and standard deviation (open circles) of the averaged extinction as a function of altitude from all 1985 and 1986 data files (11,000 profiles) without rain.

In 1986, a more accurate precipitation registration was established and the way of data processing was modified somewhat. Therefore the 1986 results (5000 profiles) were analyzed separately (for periods without precipitation). The frequency and the cumulative distributions are shown in Figures 5.26 and 5.27. In Figure 5.28, the mean and the standard deviation are presented as a function of height.

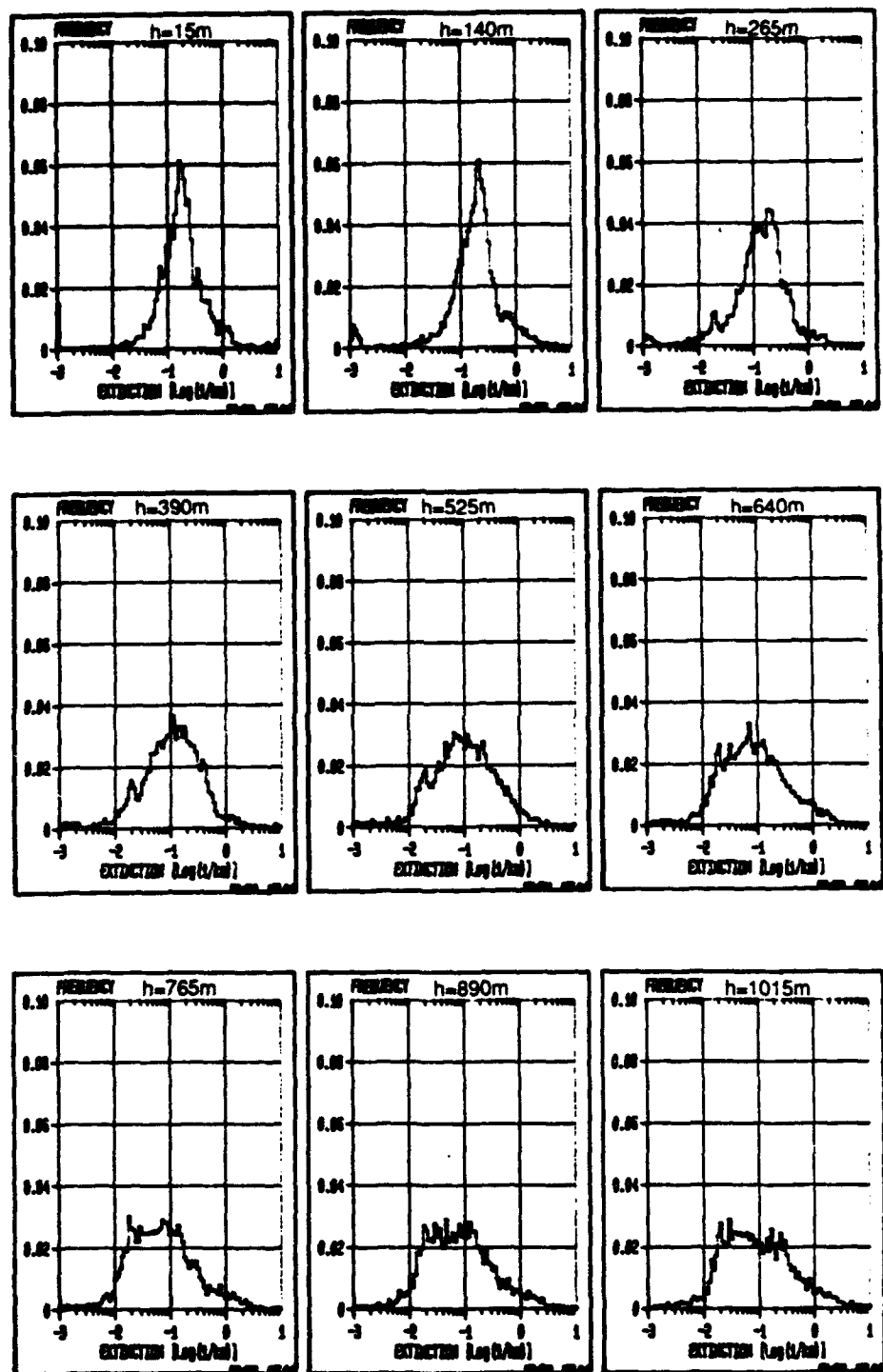


Figure 5.26: Distribution of the atmospheric extinction at nine different altitudes from the 1986 data (5000 profiles). Only periods without precipitation are selected.

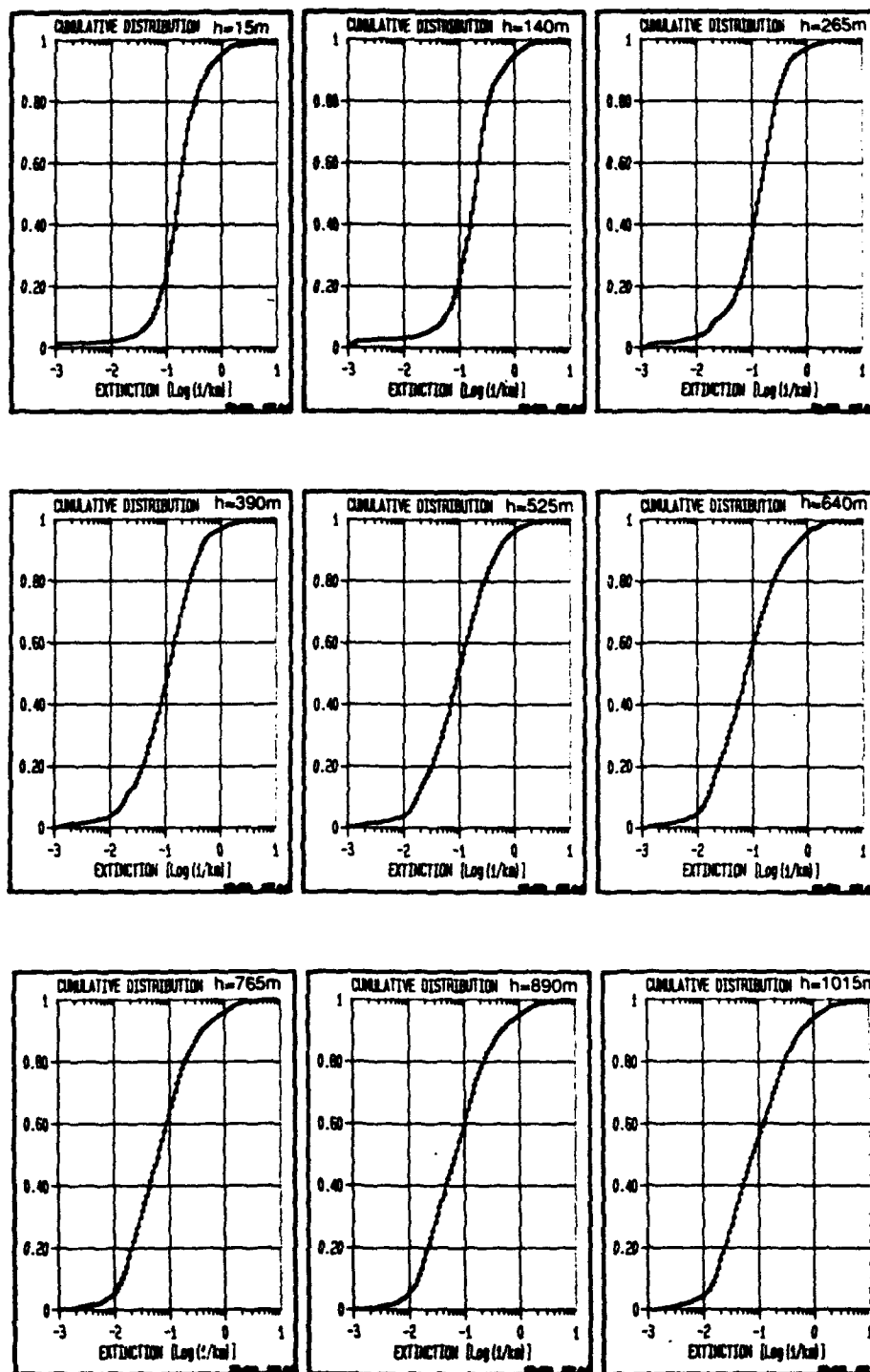


Figure 5.27: Cumulative distribution of the 1986 data at nine different altitudes. See also figure 5.25

The frequency distributions in Figure 5.26 for the low altitudes (<400 m) are different from those in Figure 5.23. Multi-modal distributions are not observed, only single mode distributions. A small spike around 10^{-3} km^{-1} corresponds to the default extinction in situations (of very good visibility) when the lidar provides a negative extinction. The peak in the frequency distribution at 15 m altitude, around 0.2 km^{-1} corresponds with the mean extinction as shown in Figure 5.1. The mean extinction shifts slowly from about 0.2 km^{-1} at 20 m altitude to about 0.08 km^{-1} at one kilometer altitude. At higher altitudes, the extinction is spread over a larger interval which extends mostly towards smaller extinction values. The averaged values and the standard deviations of the 1986 data show a somewhat similar behaviour as the combined results.

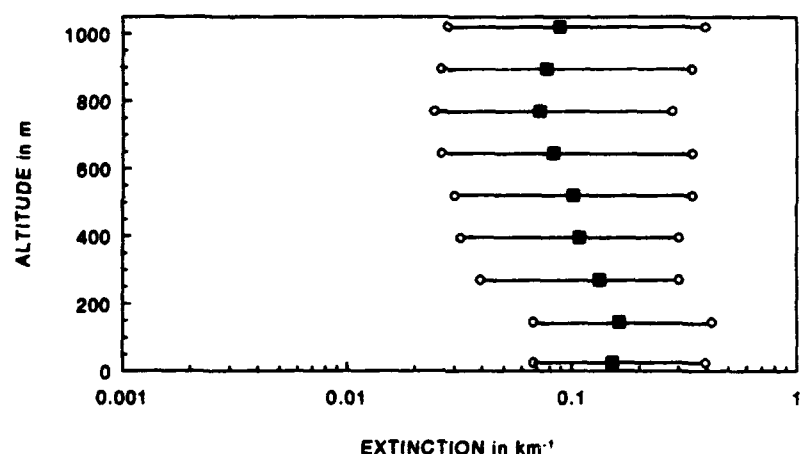


Figure 5.28: Mean (solid squares) and standard deviation (open circles) of the extinction (1986 data; 5000 profiles) as a function of altitude.

6

DISCUSSION AND CONCLUSIONS

During a period of 19 months, from January 1985 until August 1986, vertical atmospheric extinction profiles were measured with a small lidar system (optical radar) to an altitude of maximum 2000 m. The required input boundary condition, for the (forward) inversion of the signals, was measured with the same lidar system. Data has been collected continuously over periods of maximum 5 working days. After validation and combination with the actual meteo data, a data base has been established of 22,800 records.

The lidar system and the transfer functions of the electronic components were absolutely calibrated. Thus both the backscatter- and the extinction coefficients, as well as the extinction profiles, were measured quantitatively. It has been shown that the accuracy of the trigger moment of the recording system and the accuracy of the transfer function of the logarithmic amplifier play an important role, especially in situations of very low extinction coefficients. The inversion method applied has been validated during a field experiment in 1983, where aerosol and nephelometer profiles were measured simultaneously with the lidar (Lindberg et al, 1987).

The measured extinction profiles are the basic information for calculating the vertical or slant path visibility. This parameter is very important, e.g., for meteorology, aviation and for the prediction of the performance of electro-optic sensor systems. At this moment, there are no other efficient techniques to determine the vertical optical structure of the atmosphere.

Analysis of the data base has led to the following conclusions:

- It is estimated that the forward inversion method provides reliable information on the atmospheric vertical extinction profile in about 95% of the cases. Only during periods of mist or ground haze, the reverse inversion method might provide better results.
- In general, there is no fixed relation between the extinction and the backscatter coefficients. Nevertheless periods can be distinguished where a constant relation is clearly present despite the variation in the backscatter and the extinction.

- For relative humidities smaller than 90 %, both the backscatter and the extinction coefficients increase somewhat with the relative humidity. For larger values of the relative humidity, the increment is stronger but not well defined. Due to the strong variability in the measured quantities, which might be caused by different air masses, it is not possible to derive an empirical relation between relative humidity and the extinction or backscatter coefficient.
- In many cases, a 'hysteresis' loop has been observed in the relation between the backscatter coefficient and the relative humidity. We presume that this is caused by the shift in the particle size distributions in response to changes in relative humidity. For hygroscopic aerosol, these responses are different for increasing and decreasing relative humidity, resulting in a hysteresis in the growth curves (e.g., by Winkler, 1971). On the other hand, a similar behaviour has not been observed in the relation between the extinction coefficient and the relative humidity.
- In many cases, the visibility correlates both with the backscatter and with the extinction coefficients. However, there are also periods where the visibility does not correlate with either of these parameters. This depends perhaps on the type of aerosol.
- The reference values for the backscatter- and the extinction coefficients are calculated by linear regression on horizontal measurements. Calculated standard deviations in the extinction show a minimum at about 0.8 km^{-1} , and for the backscatter at about 0.02 km^{-1} , when the range of the lidar is at maximum. A more extensive study on this subject, in which the quality of the slope method has been analysed as a function of the signal-to-noise ratio and the actual extinction will be published elsewhere (Kunz and DeLeeuw, 1992).
- Analysis of a selected group (no precipitation) of profiles show that below 400 m the averaged extinction has the tendency to peak at about 0.2 km^{-1} . At higher altitudes the variation in the extinction increases, while on average the extinction coefficient decreases with height.

Recommendations for future work:

- storage of the raw lidar data is recommended (and is possible nowadays e.g. with large capacity storage media) to reprocess the data with alternative inversion algorithms.

- the inhomogeneity of the horizontal extinction- and backscatter coefficients can be expressed in the standard deviations as calculated with the slope method.
- it is desirable to extend the altitude range to 2000 m or more to increase the probability of cloud detection.
- a system, like a rain gauge, is required to indicate periods with precipitation
- a simple photodetector or a commercial pyranometer can be applied to measure the amount of background radiation (and periods of sun shine) for estimating the amount of background noise and for indicating night time periods
- the quality of logarithmic amplifiers should be investigated in more detail as regards bandwidth, noise and the transfer for small signals
- the dynamic range and the noise properties of avalanche photodiodes under different background conditions, including the applied amplifiers, should be investigated to estimate the performance of the optical receiver (Kunz and Moerman, 1992)
- the recording frequency of the meteo station (4 per hour during the project) should be adapted to the frequency of the lidar (10 per hour)
- the meteo data should not only provide the mean value per parameter over the time interval, but also the standard deviation to determine the variation (implemented at this moment)

REFERENCES

Bertolotti, M., 'Atmospheric extinction measurements of a HeNe laser'
Appl. Opt. Vol. 17, No. 2, Jan. 1978, pp 285-288

Bertolotti, M., 'On the possibility of measuring optical visibility by using a Ruby laser'
Appl. Opt., Vol. 8, No. 1, Jan. 1969, pp 117-120

Braun, C., 'General formula for the errors in aerosol properties determined from lidar
measurements at a single wavelength'
Appl. Opt., Vol. 24, No. 7, 1985, pp 925-927

De Leeuw, G., G.J. Kunz, and C.W. Lamberts, 'Humidity effects on the backscatter/extinction
ratio',
Appl. Opt., Vol. 25, No. 22, 15 Nov. 1986, pp 3971-3974

Elterman, L., 'Atmospheric attenuation model, in the ultraviolet, visible and infrared regions for
altitudes to 50 km'
AFCRL-64-740, September 1964

Hitschfeld, W. and J. Bordan, 'Errors inherent in the radar measurements of rainfall at attenuating
wavelength'
Journ. of Meteor., Vol. 11, Febr. 1954, pp 58-67

Kaestner, M., 'Lidar inversion with variable backscatter/extinctions: comment'
Appl. Opt. Vol. 25, No. 15, March 1986, pp 833-835

Klett, J.D., 'Lidar inversion with variable backscatter/extinction ratios'
Appl. Opt. Vol. 24, No. 11, 1 June 1985, pp 1638-1643

Klett, J.D., 'Stable analytical inversion solution for processing lidar returns'
Appl. Opt. Vol. 22, No. 4, 15 Febr. 1983, pp 514-515

Kohl, R.H., 'Discussion of the interpretation problem encountered in single wavelength lidar transmissometers'

Journ. of Appl. Meteor. Vol. 17, July 1978, pp 1034-1038

Kunz, G.J., 'Hidden errors in lidar-signals'

9-th International Laser Radar Conference, Munich , 2-5 July 1979

Kunz, G.J. 'The choice of digitizing lidar signals with a log-amplifier or with a high resolution A/D converter' (in Dutch)

TNO Physics and Electronics Laboratory, FEL 1990-I148

Kunz, G.J., 'Vertical atmospheric extinction profiles measured with lidar'

Appl. Opt., Vol. 22, No. 13, 1 July 1983, pp 1955-1957

Kunz, G.J., 'Introduction to and instrumentation for the vertical structure project'

TNO Physics and Electronics Laboratory, FEL 1985-30

Kunz, G.J., 'A method for measuring the vertical extinction and backscatter profile with a scanning lidar'

TNO Physics and Electronics Laboratory, FEL 1988-65

Kunz, G.J., 'Light source for testing optical receivers',

NATO AC/243 (Panel IV/RSG.8), Note NL 1988-01

Kunz, G.J., 'Light source for dynamic testing of photo receivers,

TNO Physics and Electronics Laboratory, FEL 1989-69

Kunz, G.J., 'Lidar als wolkenbasishoogte- en 'slant path' zichtmeter'

TNO Physics and Electronics Laboratory, FEL 1990-A207

Kunz, G.J., 'Cloud base monitoring with lidar'

TNO Physics and Electronics Laboratory, FEL 1990-A315

Kunz, G.J. and G. De Leeuw, 'On inversion of lidar signals with the slope method',
Accepted to Applied Optics, July 1992

Kunz, G.J. and M.M. Moerman, 'An analysis of the response and the noise of avalanche
photodiodes in combination with a pre-amplifier'
TNO Physics and Electronics Laboratory, FEL 1992-A311, in Dutch

Lamberts, C.W. and G. De Leeuw, 'Aerosol-induced visibility reduction in the Netherlands' in
Aerosols; research, risk assessment and control strategies pp. 793-807; Lewis Publishers, Inc.
Michigan, 1986 edited by Lee, S.D., T. Schneider, L.D. Grand and P.J. Verkerk,
ISBN 0-87371-051-7

Lamberts, C.W., 'Lidar: a statistical approach'
TNO Physics and Electronics Laboratory
September 1978, PhL 1978-31

Lindberg, J.D., M.G. Heaps, G.J. Kunz, and P.H. Rasmussen, 'Comparison of selected data
from the European vertical structure experiment'
NATO AC/243 (PANEL IV/RSG.8), Report 1986-2, April 1987

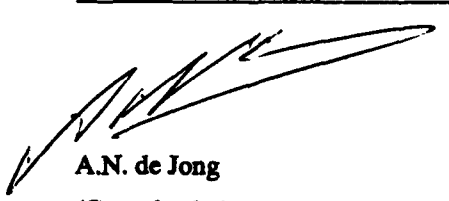
Paulson, M.R., 'Test of lidar inversion algorithm sensitivity to atmospheric backscatter and
extinction parameters'
Naval Ocean Systems Center, San Diego, USA, TD 764, January 1985

Sasano, Y., 'Error caused by using a constant A/B ratio in the lidar solution'
Appl. Opt., Vol. 24, No. 22, 1985, pp 3929-3932

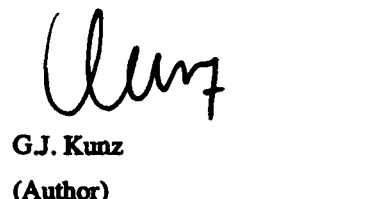
Shimuzu, H., Y Sasano, H. Nakane, N. Sugimoto, I. Matsui and N. Takeuchi, 'Large scale laser
radar for measuring aerosol distribution over wide area'
Appl. Opt., Vol. 24, No. 5, 1 March 1985, pp 617-626

Tonna, G., 'Backscattering, extinction, and liquid water content in fog: a detailed study of their
relation for use in lidar systems'
Appl. Opt., Vol. 30, No. 9, 20 March 1991, pp 1132-1140

Winkler, P. and C.E. Junge, 'Comments on: Anomalous deliquescence of sea spray aerosols'
Journ. Appl. Meteor., Vol. 10, 1971, pp 159-163



A.N. de Jong
(Groupleader)



G.J. Kunz
(Author)

APPENDIX A: RANGE OF LIDAR SYSTEMS

In this report, the range of a lidar system is defined as that range where the received power is equivalent to the noise equivalent power of the receiver. Noise is generated by the electronics and by the background radiation. In the general case of an inhomogeneous atmosphere, it is not possible to predict the maximum detection range but in the special case of a homogeneous atmosphere, this maximum range can be calculated by assuming a linear relation between the backscatter- and extinction coefficients. The starting point for the derivation of the maximum range is the common model for single scatter lidar signals from a homogeneous atmosphere. Substitution of $\alpha(R) = \alpha$, $\beta(R) = \beta$ and the noise equivalent power, P_n , for the received power in equation (3.1) leads to:

$$P_n = E_1 \cdot \frac{c}{2} \cdot \frac{\beta}{4\pi} \cdot \frac{A}{R^2 m} \cdot T_{opt} \cdot e^{-2\alpha R} \text{ m} \quad (\text{A.1})$$

where:

A	=	area of the receiver in km^2
c	=	velocity of light in km/s
E_1	=	laser energy in J
P_n	=	effective noise power of the detector in W
R_m	=	maximum range in km
T_{opt}	=	transmission of the optics
α	=	spatial extinction coefficient in km^{-1}
β	=	backscatter coefficient in km^{-1}

Taking the logarithm of (A.1) leads to:

$$2 \cdot \alpha \cdot R_m + 2 \cdot 1_n(R_m) = 1_n(K_1 \cdot \beta) \quad (\text{A.2})$$

where K_1 is the lidar system constant according to:

$$K_1' = \frac{E_1 \cdot c \cdot A \cdot T_{opt}}{2 \cdot 4 \cdot \pi \cdot P_n} \quad (A \cdot 3)$$

For a Rayleigh atmosphere at a wavelength of 1060 nm, $\alpha = 0.87 \cdot 10^{-3} \text{ km}^{-1}$ and $\beta = 1.30 \cdot 10^{-3} \text{ km}^{-1}$. Substitution of these values in (A.2) yields a maximum range for the Mini-Lidar of 450 m.

The maximum range R_{max} in a homogeneous Mie atmosphere is a function of the extinction and the backscatter. If a ratio $C_a = \beta/\alpha^k$ (generally with $k=1$) is assumed, R_{max} can be calculated by taking the total derivative of (A.2). This results in:

$$2 \cdot \alpha \cdot dR_{max} + 2 \cdot R_{max} \cdot d\alpha + \frac{2}{R_{max}} \cdot dR_{max} \frac{d\alpha}{\alpha} \quad (A \cdot 4)$$

The extinction, at which the maximum range occurs, is found by explicitly writing $dR_{max}/d\alpha$ and equating this term to zero. This results in:

$$\alpha_{R_{max}} = \frac{1}{2 \cdot R_{max}} \quad (A \cdot 5)$$

Finally, the maximum range R_{max} is found by substituting (A.5) in (A.2) where e is the base of the natural logarithm.

$$R_{max} = \left[\frac{K_1' \cdot C_a}{2 \cdot e} \right]^{1/3} \quad (A \cdot 6)$$

Equation (A.6) shows that an increase of the system power by three orders of magnitude is required to improve the range by only one order of magnitude.

Range of the Mini-Lidar:

The properties of the Mini-Lidar (after a very long time of operation) are:

$$A = 4.3 \cdot 10^{-9} \text{ km}^2$$

$$c = 3.0 \cdot 10^5 \text{ km/s}$$

$$E_1 = 50 \text{ mJ}$$

$$P_s = 8.3 \cdot 10^{-9} \text{ W}$$

$$T_{opt} = 0.5$$

Substitution of these values in (A.3) provides a value for K' :

$$K' = 154.6 \text{ km}^3$$

With $C_s = 0.07$ and formula (A.4) the maximum range is found to be 1.26 km. This range occurs when the horizontal extinction is 0.40 km^{-1} as shown by formula (A.5).

APPENDIX B: CALIBRATION OF THE LOG UNIT

The transfer of the log unit can be described by:

$$U_o = L_1 + L_2 \cdot \ln (U_i / U_r); \quad (B.1)$$

for sufficient large input signals U_i ,

where:

L_1 = constant in V

L_2 = constant in V

U_o = output voltage in V

U_i = input voltage in V

U_r = reference voltage, 1 V

The reference voltage U_r is added to make in the argument of the log function dimensionless.

The purpose of the calibration is to determine the constants L_1 and L_2 and their accuracies in the interval where the transfer is logarithmic. Therefore, a square wave test pulse with an amplitude of 4.78 V has been applied at the input of the amplifier. A passive attenuator with a range from 0-100 dB (20 dB is a factor 10 in voltage), in steps of 3 dB, is used to cover the whole input range. A second test pulse, with an amplitude of 20 % of the main test pulse and smaller in width, was added to investigate the dynamic behaviour of the transfer function. Moreover, this provided a second method to calculate the transfer function.

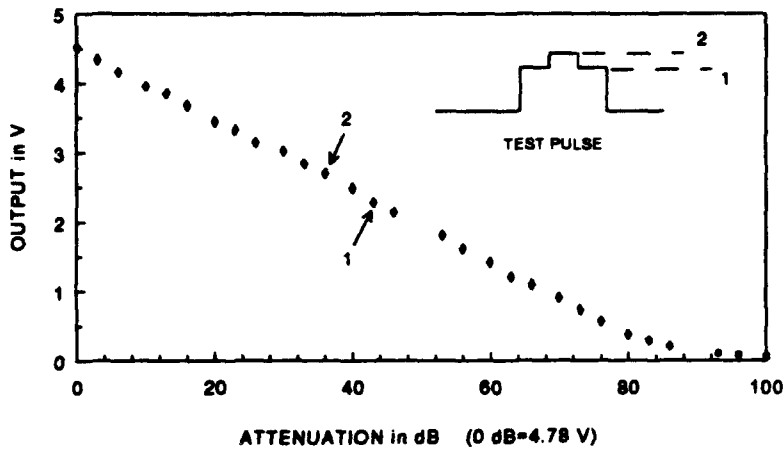


Figure B.1: Response of the log-unit as a function of the attenuator settings. The shape of the input test pulse is indicated in the figure. The lower set of data points are from the test pulse with amplitude '1'; the upper data set are from amplitude '2'.

In the range from 0 to 80 dB, the transfer is assumed to be logarithmic; in the range from 80 to 100 dB, the transfer is approximated by second order curve fitting. (Later, it appeared that for small signals the transfer becomes linear.)

The constants L_1 and L_2 are determined by linear regression analysis over the range 0 to 80 dB (25 measurement points). This provides:

$$L_1 = 377.29 \pm 1.40 \text{ V} \quad (\text{B.2a})$$

$$L_2 = 44.75 \pm 0.20 \text{ V} \quad (\text{B.2b})$$

The value of the constant L_2 can also be inverted from the additional test pulse. This can be seen by expanding (B.1) to:

$$U_o + \Delta U_o = L_1 + L_2 \cdot \ln \left[\frac{(U_i + \Delta U_i)}{U_i} \right] \quad (B.3)$$

With (B.1) this results in:

$$L_2 = \frac{\Delta U_o}{\ln \left(1 + \frac{\Delta U_i}{U_i} \right)} \quad (B.4)$$

The results are plotted in Figure B.2.

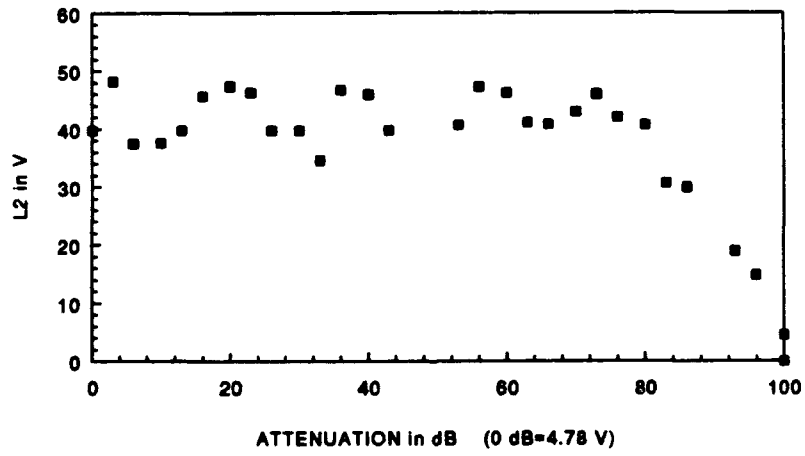


Figure B.2: Calculated value of L_2 according to equation (B.4).

Analysis of the data over the input range from 0 to 80 dB yields:

$$L_2 = 42.08 \pm 4.19 \text{ V} \quad (B.5)$$

It is clear that this method provides a similar value for L_2 as in (B.2b) but with a larger standard deviation.

- accuracy of the inverted input signals

The uncertainty in the values of L_1 and L_2 results in an inaccuracy of the inverted input signal U_i from U_o . If it is assumed that the output voltage, U_o , can be measured very accurately, than the uncertainty in the input voltage can be written as:

$$dU_i = \frac{\partial U_i}{\partial L_1} \cdot dL_1 + \frac{\partial U_i}{\partial L_2} \cdot dL_2 \quad (B \cdot 6)$$

Evaluation of the partial differentials with (B.1) results in:

$$dU_i = -\frac{U_i}{L_2} \cdot dL_1 - \frac{(U_o - L_1) \cdot U_i}{L_2^2} \cdot dL_2 \quad (B \cdot 7)$$

which leads to:

$$\frac{dU_i}{U_i} = -\frac{dL_1}{L_2} + \frac{dL_2}{L_2} \cdot \ln(U_i) \quad (B \cdot 8)$$

Substitution of the numerical values of the variables leads to the following maximum errors:

$$\frac{dU_i}{U_i} = \left| \frac{1.40}{44.75} \right| + \left| \frac{0.20}{44.75} \cdot \ln(0.0003) \right| = 0.067$$

- for an input voltage of 0.0003 V: and

$$\frac{dU_i}{U_i} = \left| \frac{1.40}{44.75} \right| + \left| \frac{0.20}{44.75} \cdot \ln(3) \right| = 0.036$$

- for an input voltage of 3 V

- transfer for very low input signals

Figure B.1 shows that for very small input signals (smaller than $5 \cdot 10^{-4}$ V) the transfer is no longer logarithmic. Therefore a second order curve has been fitted to the points from 80 dB to 100 dB. This results in the following fit

$$U_i = -0.705397 + 5.34466 \cdot U_o - 6.242335 \cdot U_o^2; \quad (B.9)$$

NOTE: The analysis thus far is based on a transfer of the log-unit for positive signals only, because negative input signals would provide unreal outputs. Later measurements showed however, that the transfer of a logarithmic amplifier is finite for very small signals. This means that a different approach is necessary as explained in Kunz, 1990.

Electrical bandwidth of the log-unit

The transfer function of the logarithmic amplifier as a function of frequency can in fact only be justified for very small input signals where the transfer is linear. Stronger input signals produce harmonics due to the logarithmic characteristics. Nevertheless, the electrical bandwidth has been determined for a number of different input levels and has been compared with a more expensive log-unit. The results, which are shown in Figure B3, indicate that the bandwidth (3 dB point) is about 6 MHz for small signals and increases slightly to 8 MHz for large input signals. The slope is about 12 dB per octave which means that signals with high frequency components are strongly attenuated. (A log-unit from a different supplier indicated a bandwidth of better than 20 MHz with a slope of less than 2 dB per octave).

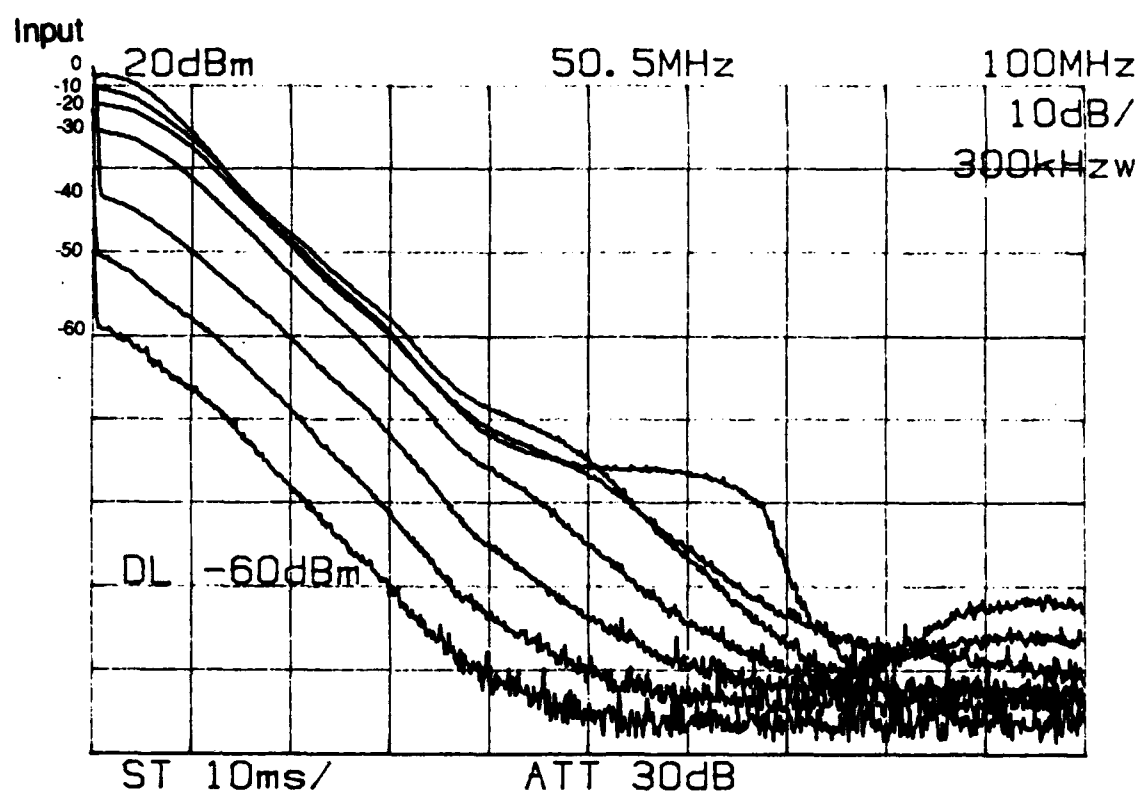


Figure B.3: Frequency response of the logarithmic amplifier LA-90-P at different input levels. The frequency is along the horizontal axis (0..100 MHz) and the vertical axis represents the response in dB's.

APPENDIX C: EFFECTS OF THE TRIGGER INACCURACY

The purpose of lidar is, among others, to measure the extinction and the backscatter profiles in the atmosphere as a function of range. However, the signals decrease with the square of the range. This is called 'geometric attenuation'. It is common practice, to start signal processing with compensating for this geometric attenuation. The moment that the laser pulse is emitted is the reference for the starting point of this process. However, if no special precautions are taken, there is always an uncertainty of maximum one sample interval. From the viewpoint of signal processing, the signal is corrected with $(R+\Delta R)^2$ in stead of with R^2 . The influence of this error on the calculated extinction- and backscatter coefficients is discussed in this section.

Because it is not possible to treat all possible inhomogeneous situations, only signals from homogeneous atmospheres are considered. Furthermore, this analysis should only be considered as a first step to quantify this problem.

For simplicity, it is assumed that the lidar signal can be described with the following simplified model:

$$P_d(R) = \frac{K_1 \cdot \beta \cdot e^{-2\alpha R}}{R^2} \quad (C \cdot 1)$$

where:

K_1 = lidar system constant in $\text{W} \cdot \text{km}^3$
 $P_d(R)$ = received power in W
 R = range in km
 α = extinction coefficient in km^{-1}
 β = backscatter coefficient in km^{-1}

If there is a shift in the trigger moment, than the range correction is performed with an additional unknown shift ΔR . This can be described as:

$$S(R) = P(R) \cdot (R \pm \Delta R)^2, \quad (C \cdot 2)$$

where $S(R)$ is the range corrected lidar signal in $\text{W} \cdot \text{km}^2$.

If $\Delta R=0$, than both the extinction and the backscatter can be determined from a linear regression fit on $\text{LN}[S(R)]$. However, if ΔR is not equal to zero, the application of linear regression to determine the errors in the calculated extinction- and backscatter coefficients leads to very complicated analysis. Therefore, the problem is split into two parts:

- determine the error in the backscatter assuming that the extinction is known
- determine the error in the extinction assuming that the backscatter is known

Error in the inverted backscatter

The backscatter coefficient is determined by averaging over interval R_1 to R_2 according to:

$$\beta \pm \Delta \beta = \frac{1}{(R_2 - R_1)} \cdot \int_{R_1}^{R_2} \frac{P_d(R) \cdot (R \pm \Delta R)^2}{K_1 \cdot e^{-2 \cdot \alpha \cdot R}} \cdot dR \quad (C \cdot 3)$$

For small values of $\Delta R/R$, the quadratic term is approximated by the first term of the series expansion. Than the integral leads to:

$$\frac{\Delta \beta}{\beta} = \frac{2 \cdot \Delta R}{(R_2 - R_1)} \cdot \text{LN} \left[\frac{R_2}{R_1} \right] \quad (C \cdot 4)$$

Thus the error in the backscatter is proportional to the trigger inaccuracy and depends also on the position and the length of the selected interval.

Appendix C

For example, a trigger inaccuracy of 30 ns leads to an error of about 1.2 % in the backscatter ($R_1=100$ m and $R_2=1000$ m). The error increases to about 3.1 % if R_2 is 200 m.

Error in the inverted extinction

The error in the extinction is determined by comparing the average slope of the selected interval with the actual extinction coefficient. Furthermore, it is assumed that the backscatter β is known. Then one can write:

$$\alpha \pm \Delta\alpha = \frac{1}{(R_2 - R_1)} \cdot \int_{R_1}^{R_2} \frac{-d}{2 \cdot dR} \cdot \ln \left[\frac{P_d(R \pm \Delta R)^2}{\beta \cdot K_1} \right] \cdot dR \quad (C \cdot 5)$$

For small values of $\Delta R/R$, the quadratic term can be approximated by the first term of the series expansion. Subsequent evaluation of the integral leads to the following relative error in the extinction:

$$\frac{\Delta\alpha}{\alpha} = \frac{\Delta R}{\alpha \cdot R_1 \cdot R_2} \quad (C \cdot 6)$$

For example, if the trigger inaccuracy is 30 ns and the measurement is made in a clear atmosphere with $\alpha = 0.1 \text{ km}^{-1}$, the error in the extinction becomes 56 % when $R_1 = 100$ m and $R_2 = 800$ m!

APPENDIX D: EFFECTS OF THE TRANSFER ACCURACY OF THE LOG UNIT

The uncertainty of the transfer of the log unit leads to errors in the calculated extinction- and backscatter coefficients. For simplicity, only signals from homogeneous atmospheres are considered. The problem is split in two parts:

- calculate the influence on the extinction, assuming that the backscatter is known
- calculate the influence on the backscatter, assuming that the extinction is known

The analysis starts with the simplified model of the lidar equation from homogeneous atmospheres:

$$U_1(R) = \frac{K_1 \cdot D \cdot \beta}{R^2} \cdot e^{-2\alpha \cdot R} \quad (D \cdot 1)$$

were:

D	=	sensitivity of the detector in V/W
K ₁	=	lidar system constant in W·km ³
R	=	range in km
α	=	extinction coefficient in km ⁻¹
β	=	backscatter coefficient in km ⁻¹

According to equation (B.1), the output of the log unit becomes:

$$U_o(R) = L_1 + L_2 \cdot [LN(K_1 \cdot D \cdot \beta) - 2 \cdot \alpha \cdot R - 2 \cdot LN(R)] \quad (D \cdot 2)$$

Note that the reference voltage has been set to U_r = 1 V and will therefore not appear in this

equation.

The extinction coefficient α can explicitly be written as:

$$\alpha = \frac{\ln(K_1 \cdot D \cdot \beta) - 2 \cdot \ln(R) - \frac{(U_0 - L_1)}{L_1}}{2 \cdot R} \quad (D.3)$$

Now the total error in the extinction, due to errors in the transfer constants of the log unit, can be written as:

$$d\alpha = \frac{\partial \alpha}{\partial L_1} \cdot dL_1 + \frac{\partial \alpha}{\partial L_2} \cdot dL_2 \quad (D.4)$$

with:

$$\frac{\partial \alpha}{\partial L_1} = \frac{1}{2 \cdot R \cdot L_2} \quad (D.5a)$$

and

$$\frac{\partial \alpha}{\partial L_2} = \frac{\ln(U_1)}{2 \cdot R \cdot L_2} \quad (D.5b)$$

The total error in the extinction becomes:

$$d\alpha = \frac{1}{2 \cdot R \cdot L_2} \cdot dL_1 + \frac{\ln(U_1)}{2 \cdot R \cdot L_2} \cdot dL_2 \quad (D.6)$$

The average error in the extinction over interval R_1 to R_2 becomes:

$$\Delta\alpha = \frac{1}{(R_2 - R_1)} \cdot \int_{R_1}^{R_2} \left[\frac{\Delta L_1}{2 \cdot R \cdot L_2} + \frac{\ln(U_1) \cdot \Delta L_2}{2 \cdot R \cdot L_2} \right] \cdot dR \quad (D.7)$$

After evaluating expression (D.7) one finds:

$$\Delta\alpha = \frac{\Delta L_1 \cdot \ln\left(\frac{R_2}{R_1}\right) + \Delta L_2 \cdot \left[\ln(K_1 \cdot D \cdot \beta) \cdot \ln\left(\frac{R_2}{R_1}\right) - 2 \cdot \left[\ln\left(\frac{R_2}{R_1}\right) \right]^2 - 2 \cdot \alpha \cdot (R_2 - R_1) \right]}{2 \cdot L_2 \cdot (R_2 - R_1)} \quad (D.8)$$

The relative uncertainty in α has been calculated by substituting the values of K_i , D , L_1 , ΔL_1 , L_2 , ΔL_2 and the relation of β/α in (D.8). (See Table 2.1 and Appendix B; for β/α a value of 0.07 has been substituted). For R_1 a value of 0.1 km has been chosen and for R_2 a value of 1 km. The relative uncertainty in the extinction, $\Delta\alpha/\alpha$, due to uncertainty in L_1 and L_2 only, amounts -385 %, -23.1 % and -1.33 %, for α values of 0.01 km^{-1} , 0.1 km^{-1} and 1.0 km^{-1} respectively. These calculations show that it is difficult to measure small extinction values with this log unit (and this small lidar system). Moderate and large extinctions can be measured more accurately. Note that the uncertainty can be even worse if the detector noise, the spatial variation of the atmospheric scattering and the uncertainty in the other parameters are taken into account.

In the same way the error in the backscatter coefficient is calculated, assuming that the extinction coefficient is known.

$$d\beta = \frac{\partial \beta}{\partial L_1} \cdot dL_1 + \frac{\partial \beta}{\partial L_2} \cdot dL_2 \quad (\text{D} \cdot 9)$$

with:

$$\frac{\partial \beta}{\partial L_1} = \frac{-1}{L_2} \cdot \beta \quad (\text{D} \cdot 10\text{a})$$

and

$$\frac{\partial \beta}{\partial L_2} = \frac{-\text{LN}(U_1)}{L_2} \cdot \beta \quad (\text{D} \cdot 10\text{b})$$

The total uncertainty in the backscatter coefficient becomes:

$$d\beta = \frac{-\beta}{L_2} \cdot dL_1 - \frac{\beta \cdot \text{LN}(U_1)}{L_2} \cdot dL_2 \quad (\text{D} \cdot 11)$$

The averaged error in the backscatter over interval R_1 to R_2 becomes:

$$\Delta\beta = \frac{-\beta}{(R_2 - R_1)} \cdot \int_{R_1}^{R_2} \left[\frac{1}{L_2} \cdot \Delta L_1 + \frac{\ln(U_1)}{L_2} \cdot \Delta L_2 \right] \cdot dR \quad (D.12)$$

After evaluating expression (D.12) the absolute uncertainty in the backscatter becomes:

$$\Delta\beta = -\beta \cdot \left[\frac{\Delta L_1}{L_2} + \frac{\Delta L_2}{L_2} \cdot \left\{ \ln(K_1 \cdot D \cdot \beta) - \alpha \cdot (R_2 + R_1) - 2 - 2 \cdot \frac{R_2 \cdot \ln(R_2) - R_1 \cdot \ln(R_1)}{(R_2 - R_1)} \right\} \right] \quad (D.13)$$

The relative uncertainty in the backscatter has been calculated with the same system values as described under (D.8). This results in an uncertainty of 1.32 % in $\Delta\beta/\beta$ if the extinction is 0.01 km^{-1} . For extinctions of respectively 0.1 and 1.0 km^{-1} the relative uncertainty is 1.9 % and 2.9 %.

Conclusion

The uncertainty in the transfer function of the applied log-amplifier has only a slight influence on the calculated backscatter. The influence on the calculated extinction is much stronger and increases as the extinction decreases. Uncertainties as large as a factor 3 are possible if the extinction is 0.01 km^{-1} .

APPENDIX E: DEFINITION OF THE PARAMETERS IN THE DATA BASE

The following parameters are present in the final data base:

- 1 - lidar date
- 2 - meteo time
- 3 - lidar time
- 4 - number of lidar reference measurements
- 5 - meteo date
- 6 - sampling interval lidar
- 7 - meteo code
- 8 - attenuator
- 9 - cloud detection on/off
- 10 - temperature
- 11 - dewpoint
- 12 - relative humidity
- 13 - lidar elevation angle
- 14 - pressure
- 15 - wind velocity
- 16 - wind direction
- 17 - visibility AEG
- 18 - radon counter
- 19 - transmission over 265 m
- 20 - minimum value profile
- 21 - maximum value profile
- 22 - min. altitude profile
- 23 - max. altitude profile
- 24 - laser energy
- 25 - horizontal extinction in km^{-1}
- 26 - horizontal backscatter in km^{-1}
- 27 - horizontal delta extinction in km^{-1}
- 28 - horizontal delta backscatter in km^{-1}
- 29 - turbulence
- 30 - cloud cover
- 31 - running averaged extinction
- 32 - running averaged backscatter
- 33 - altitude reliability??
- 34 - cloud altitude in m
- 35 - cloud thickness in m

APPENDIX F: SOME RESULTS OF THE SODAR SYSTEM

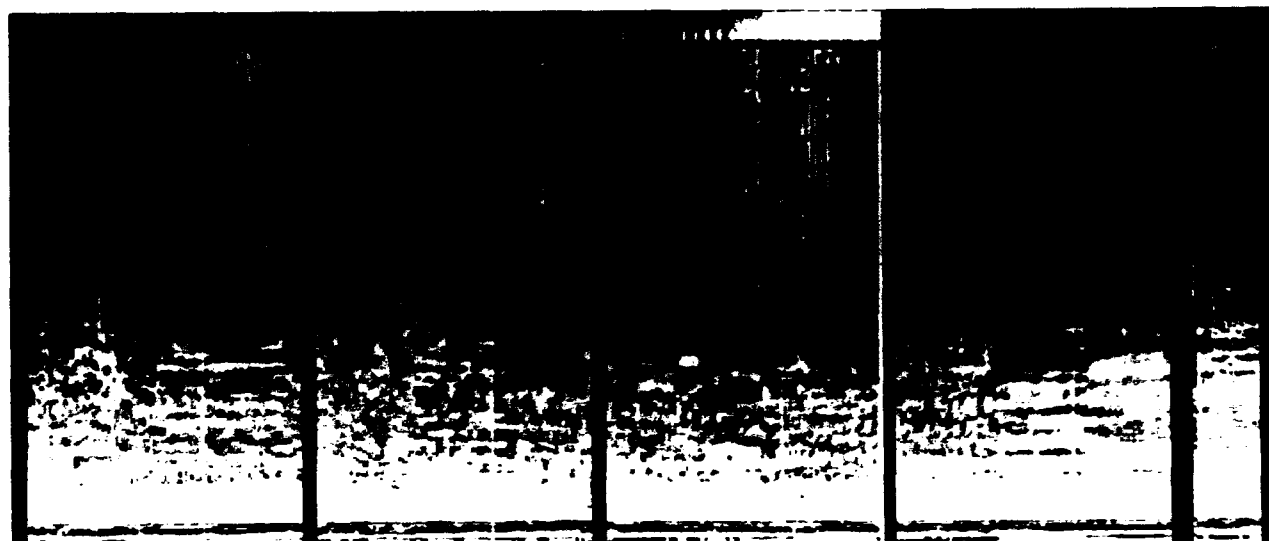
In 1984 and 1985, an experimental sodar system has been constructed with a high-power speaker and a parabolic disk with a diameter of about 60 cm. The transmitter operated at a frequency of 1650 Hz with an acoustic power of 50 W. The sodar system was mounted on the roof of the institute at an altitude of about 15 m above ground level. A small wooden cylinder around the system should suppress the background noise. The bandwidth of the receiver was about 40 Hz which was realized with a boxcar integrator. A PET 2000 Commodore Business Computer controlled the system and the data were stored on audio cassette tape which had a storage capacity of about 100 signals. Therefore each sodar profile presented here is an average of about 15 minutes.

Some of the obtained sodar data are presented in Figure F.1. Here the received power has been coded in false color in a time versus height diagram. The vertical axis represents the height from 15 to 415 m whereas the time has been plotted along the horizontal axis. The hourly intervals have been indicated by the small vertical tics at the bottom and the top of the figure.

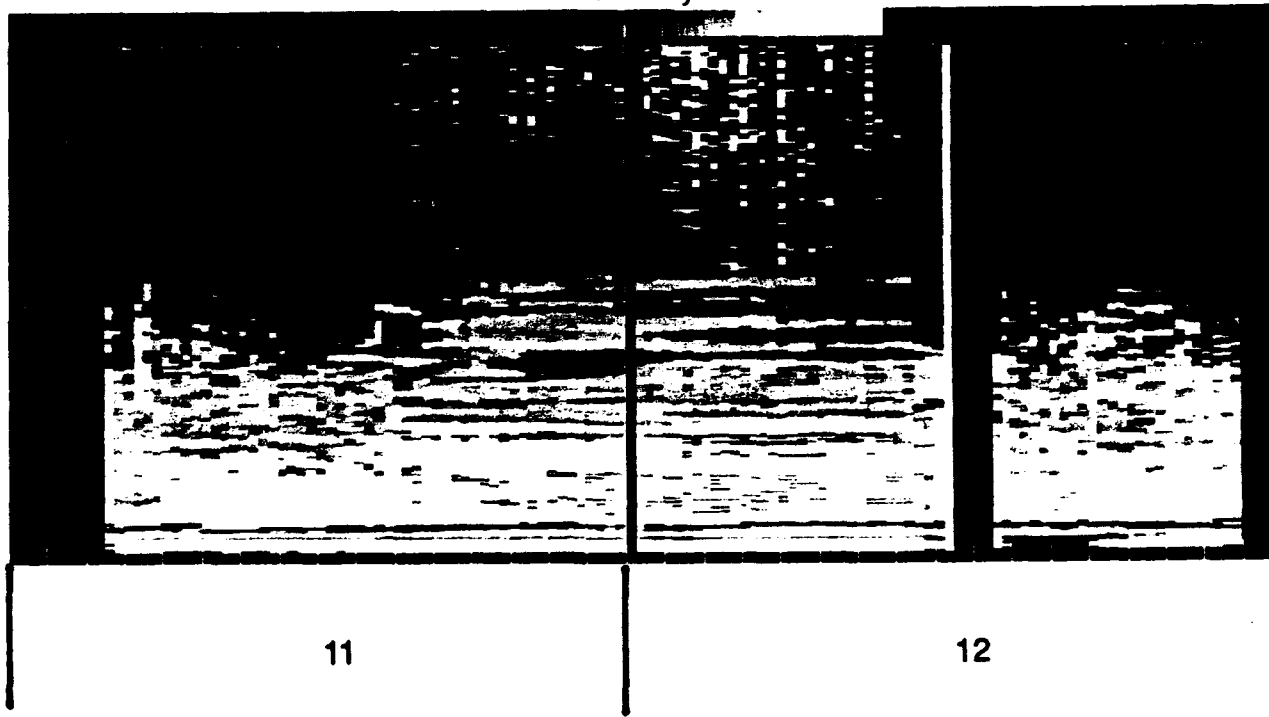
Two different time intervals can be distinguished viz. from 07:00 a.m. to 07:00 p.m. and from 07:00 p.m. to 07:00 a.m. As in many other data files, the data show much structure during the day from about 07:00 a.m., when the laboratory opens, until 06:00 p.m. when the laboratory closes. It is conjectured therefore, that the measured structure is not only caused by thermal effects but also by the background noise of, e.g., the engines of cars and other human activities. During the evening and the night, the background noise is at a lower level and some horizontal structure becomes visible between about 50 m and 300 m altitude.

The results of a two days period, which are shown in Figure F.1b, show similar effects. The horizontal layering is clearly visible during the night but disappears here after 07:00 a.m.

The sodar results do not show any correlation with the lidar results. This can partly be explained from the different interaction processes and the limited range of the sodar system. For possible future sodar work, it is recommended to have a better acoustic isolation from the environment and a more sensitive system.



February 1985



February 1985

Figure F.1: Vertical structure of the atmosphere, coded in false color, as measured with an acoustic sounder (sodar). Vertical axis 0-400 m; horizontal axis is time: the small vertical lines indicate the hourly interval and the large vertical lines indicate midnight. Sodar results from February 4 to 8, 1985, (a) and sodar results from February 11 to 12, 1985 (b).

REPORT DOCUMENTATION PAGE**(MOD-NL)**

1. DEFENSE REPORT NUMBER (MOD-NL)	2. RECIPIENT'S ACCESSION NUMBER	3. PERFORMING ORGANIZATION REPORT NUMBER
TD93-0756		FEL-93-A058
4. PROJECT/TASK/WORK UNIT NO.	5. CONTRACT NUMBER	6. REPORT DATE
22392	A90K703	AUGUST 1993
7. NUMBER OF PAGES	8. NUMBER OF REFERENCES	9. TYPE OF REPORT AND DATES COVERED
78 (INCL. 6 APPENDICES, EXCL. RDP & DISTRIBUTION LIST)	29	
10. TITLE AND SUBTITLE		
RESULTS FROM THE VISA PROJECT		
11. AUTHOR(S)		
G.J. KUNZ		
12. PERFORMING ORGANIZATION NAME(S) AND ADDRESS(ES)		
TNO PHYSICS AND ELECTRONICS LABORATORY, P.O. BOX 96864, 2509 JG THE HAGUE Oude Waalsdorperweg 63, THE NETHERLANDS		
13. SPONSORING/MONITORING AGENCY NAME(S)		
ROYAL NETHERLANDS NAVY, DMKM/WCS/COSPON		
14. SUPPLEMENTARY NOTES		
THE CLASSIFICATION DESIGNATION ONGERUBRICEERD IS EQUIVALENT TO UNCLASSIFIED.		
15. ABSTRACT (MAXIMUM 200 WORDS, 1044 POSITIONS)		
A SMALL LIDAR SYSTEM HAS BEEN USED TO MEASURE THE VERTICAL STRUCTURE OF THE ATMOSPHERIC EXTINCTION IN A DUNE AREA BORDERING THE HAGUE (THE NETHERLANDS), AT ABOUT 2.6 KM FROM THE NORTH SEA. THE ATMOSPHERIC OPTICAL PROPERTIES AT THIS LOCATION ARE DETERMINED BY A MIXTURE OF INDUSTRIAL, URBAN, RURAL AND MARINE AEROSOLS, WHICH COMPOSITION DEPENDS ON THE AIR MASS HISTORY. THE MEASUREMENTS WERE MADE UNATTENDED, AROUND THE CLOCK, FIVE DAYS A WEEK. ABOUT 250 EXTINCTION PROFILES WERE RECORDED EVERY DAY. THIS REPORT REVIEWS THE DATA BASE OBTAINED AND PRESENTS SOME SELECTED RESULTS. THE LIDAR SYSTEM IS DESCRIBED BRIEFLY. FACTORS INFLUENCING THE ACCURACY OF THE INVERSION OF LIDAR SIGNALS ARE DISCUSSED.		
16. DESCRIPTORS	IDENTIFIERS	
OPTICAL RADER (LIDAR) VISIBILITY VARIATION WITH HEIGHT EXTINCTION MEASUREMENT	SIGNAL INVENSION VERTICAL EXTINCTION PROFILES	
17a. SECURITY CLASSIFICATION (OF REPORT) ONGERUBRICEERD	17b. SECURITY CLASSIFICATION (OF PAGE) ONGERUBRICEERD	17c. SECURITY CLASSIFICATION (OF ABSTRACT) ONGERUBRICEERD
18. DISTRIBUTION/AVAILABILITY STATEMENT	17d. SECURITY CLASSIFICATION (OF TITLES) ONGERUBRICEERD	
UNLIMITED		